New Mexico Geological Society

Downloaded from: https://nmgs.nmt.edu/publications/guidebooks/76



Authigenic Carbonate and Organic Carbon Stable-Isotope Constraints on Paleoenvironments and Climate in the Albuquerque Basin During the Neogene

Jeremy K.C. Rugenstein, Rachel E. Bernstein, Adam C. Walsh, Matthew Heizler, and Daniel J. Koning

2026, pp. 301-318. https://doi.org/10.56577/FFC-76.301

in:

Geology of the Albuquerque Region - Fall Field Conference 2026, Connell, Sean D.; Koning, Daniel J.;, New Mexico Geological Society 76th Annual Fall Field Conference Guidebook, 452 p. https://doi.org/10.56577/FFC-76

This is one of many related papers that were included in the 2026 NMGS Fall Field Conference Guidebook.

Annual NMGS Fall Field Conference Guidebooks

Every fall since 1950, the New Mexico Geological Society (NMGS) has held an annual Fall Field Conference that explores some region of New Mexico (or surrounding states). Always well attended, these conferences provide a guidebook to participants. Besides detailed road logs, the guidebooks contain many well written, edited, and peer-reviewed geoscience papers. These books have set the national standard for geologic guidebooks and are an essential geologic reference for anyone working in or around New Mexico.

Free Downloads

NMGS has decided to make peer-reviewed papers from our Fall Field Conference guidebooks available for free download. This is in keeping with our mission of promoting interest, research, and cooperation regarding geology in New Mexico. However, guidebook sales represent a significant proportion of our operating budget. Therefore, only *research papers* are available for download. *Road logs*, *mini-papers*, and other selected content are available only in print for recent guidebooks.

Copyright Information

Publications of the New Mexico Geological Society, printed and electronic, are protected by the copyright laws of the United States. No material from the NMGS website, or printed and electronic publications, may be reprinted or redistributed without NMGS permission. Contact us for permission to reprint portions of any of our publications.

One printed copy of any materials from the NMGS website or our print and electronic publications may be made for individual use without our permission. Teachers and students may make unlimited copies for educational use. Any other use of these materials requires explicit permission.

This page is intentionally left blank to maintain order of facing pages.

New Mexico Geological Society Guidebook, 76th Fall Field Conference, 2026, p. 301–317, https://doi.org/10.56577/FFC-76.301

AUTHIGENIC CARBONATE AND ORGANIC CARBON STABLE-ISOTOPE CONSTRAINTS ON PALEOENVIRONMENTS AND CLIMATE IN THE ALBUQUERQUE BASIN DURING THE NEOGENE

JEREMY K.C. RUGENSTEIN[1], RACHEL E. BERNSTEIN[1], ADAM C. WALSH[1], MATTHEW HEIZLER[2], AND DANIEL J. KONING[2]

[1]Department of Geosciences, Colorado State University, Fort Collins, CO 80523 USA; jeremy.rugenstein@colostate.edu
[2]New Mexico Bureau of Geology and Mineral Resources, Socorro, NM

Abstract—Model projections of future climate in central New Mexico remain uncertain. Major sources of uncertainty include how the seasonality of precipitation will change in response to warming and how plant communities will respond to changing CO_2 levels, temperatures, and precipitation seasonality. Plants and the seasonality of precipitation influence surface discharge and infiltration during precipitation events. Paleosol, and to a lesser extent shallow-groundwater, authigenic carbonate $\delta^{18}O$ and $\delta^{13}C$ are sensitive to changes in precipitation seasonality, plant community composition, and vegetation productivity. This study uses authigenic carbonate $\delta^{18}O$ and $\delta^{13}C$ from lower Miocene through lower Pliocene strata of the Santa Fe Group in the northwestern Albuquerque Basin to constrain precipitation seasonality and landscape-scale, primary plant productivity over a long period of global cooling and CO_2 decline. Using new and preexisting age control, we constrain the ages of these stratigraphic intervals to 20–17.0 Ma, 14.8–12.0 Ma, 7.2–6.4(?) Ma, and 5.0–4(?) Ma. The first two periods bracket the middle Miocene Climatic Optimum. The 5.0–4(?)-Ma period is notable because it corresponds to the development of the Rincones paleosurface and to a prolonged period of local relative landscape stability and calcic paleosol development in the northwestern Albuquerque Basin. Authigenic carbonate $\delta^{18}O$ values increase starting in the middle Miocene and reach the highest average values in the Pliocene. We find that $\delta^{13}C$ values were low ($\delta^{13}C$ −4.5 to −5.5) during the 20–17-Ma and 14–12-Ma intervals and relatively higher during 14.8–14.0 Ma ($\delta^{13}C$ −4.0 to −4.5). Notably, there is an ~1.5‰ increase in paleosol carbonate $\delta^{13}C$ between the early–middle Miocene (~17–15 Ma) and latest Miocene. To determine whether this shift was driven by the appearance of C_4 vegetation, we analyzed a late Miocene subset of these data for organic carbon $\delta^{13}C$. These organic carbon $\delta^{13}C$ values (mean of –23.6 ± 0.9‰) are likely too low to be indicative of primarily C_4 vegetation, though our data do not preclude the presence of some C_4 plants in the late Miocene. Further, the increase in paleosol carbonate $\delta^{13}C$ is opposite to the trend expected if atmospheric pCO_2 was the primary control on paleosol carbonate $\delta^{13}C$. Although our new stable-isotope record is not continuous, we interpret it as reflective of paleoclimate, with an ongoing shift toward summertime moisture in the late Neogene and the increase in $\delta^{13}C$ reflective of long-term drying and consequent de-greening of the landscape in the Albuquerque Basin. The organic carbon $\delta^{13}C$ values support this interpretation, suggesting a semi-arid climate in the latest Miocene without widespread C_4 grasses and with high water-use efficiency imparting a lower fractionation between atmospheric CO_2 and plant matter organic carbon. Authigenic carbonate $\delta^{13}C$ values and estimated plant productivity increased in the early Pliocene compared to 7.2–6.4(?) Ma, consistent with higher vegetative cover during formation of the prominent petrocalcic paleosol developed on the Rincones paleosurface.

INTRODUCTION

Projections of future climate in New Mexico as atmospheric CO_2 and global temperatures rise remain uncertain (Seager and Vecchi, 2010; Schmidt and Grise, 2021; Simpson et al., 2021). Part of this uncertainty arises from the dual wet-season hydroclimate of the region, which experiences a brief monsoon (the North American Monsoon) during July, August, and September that sources moisture from the Gulfs of Mexico and California and also receives moisture during the winter months from the mid-latitude westerlies (Sheppard et al., 2002). How each of these circulation systems will respond to rising atmospheric CO_2 is unclear, and the uncertainty in model projections encompasses both increases and decreases in precipitation (Schmidt and Grise, 2021; Alessi and Rugenstein, 2024). A second source of uncertainty arises from changes in vegetation that modify the amount of water available on the landscape. Evapotranspiration is expected to increase in the U.S. Southwest as temperatures rise (Milly and Dunne, 2020; Overpeck and Udall, 2020) and as rising CO_2 fertilizes plants, driving an increase in leaf area and water use (Mankin et al., 2017). As a consequence, runoff is projected to decrease, although the magnitude of this decrease is highly dependent upon landscape-scale ecosystem changes.

In this paper, we use the stable isotopes of oxygen ($\delta^{18}O$) and carbon ($\delta^{13}C$) preserved in authigenic carbonates to address these two uncertainties and constrain how climate in New Mexico changed in response to higher atmospheric CO_2 and the globally warmer temperatures during the Miocene. We take advantage of the exposure of Miocene terrestrial sediments hosted within the Santa Fe Group in the northwestern Albuquerque Basin (Fig. 1; Tedford and Barghoorn, 1999). The Santa Fe Group is the siliclastic basin fill of the Rio Grande rift and, in the study area, lies unconformably on the Cretaceous Menefee Formation and Paleogene Galisteo Formation. The Santa Fe Group spans the early Miocene to the early Pleistocene. Although eolian sedimentation is widely present ~20–18 Ma, fluvial strata dominate during the rest of the Miocene (Koning et al., in press). These fluvial strata are mostly associated with broad, sandy fans associated with ephemeral(?) paleodrainages sourced in the southeastern Colorado Plateau (Koning et al., in press). Throughout this succession,

there are abundant authigenic carbonates, including carbonates that formed within paleosols (i.e., nodules, rhizoliths, and root casts) and groundwater carbonates that reflect cementation during shallow groundwater flow. The oxygen ($\delta^{18}O$) and carbon ($\delta^{13}C$) isotopes of these authigenic carbonates have long been used to constrain paleoclimates, both in New Mexico (Mack et al., 1994; Jochems and Morgan, 2018; Spaur et al., 2025) and across the western United States (Winnick et al., 2013; Mix et al., 2013; Manser et al., 2024). Carbonate $\delta^{13}C$ has been used to reconstruct landscape-scale productivity to understand the evolution of paleoenvironments as climate and tectonics change (Takeuchi et al., 2010; Caves et al., 2014, 2016a; Rugenstein and Chamberlain, 2018; Licht et al., 2020).

Herein, we use authigenic carbonate $\delta^{18}O$ and $\delta^{13}C$ to reconstruct sources of moisture and plant productivity in the Albuquerque Basin over three time periods in the Miocene (one each in the early, middle, and late Miocene) and one in the early Pliocene. There appears to be a small increase in $\delta^{13}C$ in the latest Miocene relative to the middle Miocene that we attribute to declining plant productivity as the world cooled (Herbert et al., 2016; Westerhold et al., 2020; Steinthorsdottir et al., 2021). In contrast, $\delta^{18}O$ appears to continuously increase

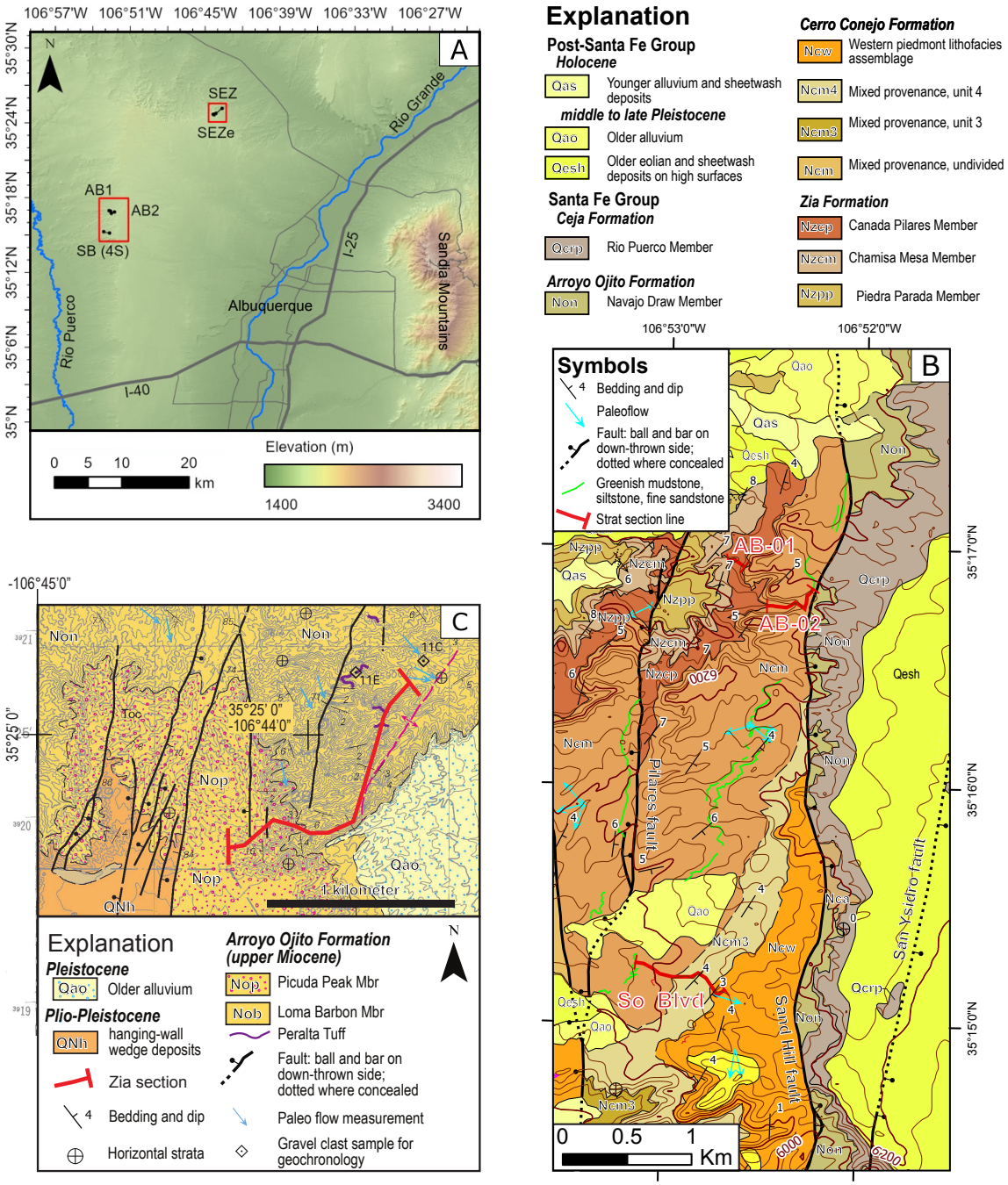


FIGURE 1. Location of the stratigraphic sections presented in this study. A) Overview of the Albuquerque region. Black dots show the bottom and top of each section and red boxes outline the areas shown in panels B and C. B) Geologic map of the AB1, AB2, and SB stratigraphic sections along the Ceja del Rio Puerco (geologic map adapted from Koning et al., in press). C) Geologic map of the SEZ and SEZ-ext sections, modified slightly from Koning and Personius (2002).

starting in the middle Miocene. These records suggest a decline in wintertime precipitation (Spaur et al., 2025) associated with Neogene cooling and opening of the Gulf of California, which provides abundant moisture to the modern-day North American Monsoon (Johnson and Delworth, 2022). This record provides a complement to long-term stable-isotope records of climate from the Española Basin (Spaur et al., 2025; Bernstein et al., 2026), thereby strengthening base-wide Rio Grande rift paleoclimate comparisons.

APPROACH

The $\delta^{18}O$ of authigenic carbonate in the southwestern United States is frequently used to reconstruct moisture sources (Wagner et al., 2010; Asmerom et al., 2010; Winnick et al., 2013; Manser et al., 2024; Spaur et al., 2025). Wintertime precipitation typically has low $\delta^{18}O$, reflecting both low specific humidity and moisture sourced from the Pacific Ocean that traverses high topography to the west. In contrast, the $\delta^{18}O$ in summertime precipitation is typically high, reflective of high specific humidity and moisture sourced from the Gulf of California, Gulf of Mexico, and subtropical Pacific Ocean and plant transpiration to the south (Strong et al., 2007; Hu and Dominguez, 2015; Dominguez et al., 2016), all of which tend to produce high precipitation $\delta^{18}O$ (Tulley-Cordova et al., 2021; Spaur et al., 2025). This precipitation $\delta^{18}O$ signal has been used to track the seasonality of precipitation in the past: low carbonate $\delta^{18}O$ is thought to reflect a greater contribution of wintertime moisture, whereas high carbonate $\delta^{18}O$ reflects more summertime precipitation (Asmerom et al., 2010; Wagner et al., 2010; Bhattacharya et al., 2022; Spaur et al., 2025).

The $\delta^{13}C$ of authigenic carbonates has been used to trace a variety of paleoenvironmental parameters. The carbon isotope composition of paleosol carbonates reflects the competing influences of (1) the partial pressure of atmospheric CO_2, (2) the partial pressure of soil-respired CO_2, and (3) the $\delta^{13}C$ of each of these sources of CO_2 (Cerling and Quade, 1993; Cerling, 1999; Caves et al., 2016a). Equation 1 shows the relationship between soil carbonate $\delta^{13}C$ and these parameters.

$$\delta_s = \frac{\left(\frac{C_a}{C_s}\right)\delta_a + 1.0044\delta_o + 4.4}{1+\left(\frac{C_a}{C_s}\right)} \quad (1),$$

where δ_a, δ_o, and δ_s are the $\delta^{13}C$ of atmospheric CO_2, CO_2 sourced from respiration of root and soil organic matter, and soil CO_2, respectively; C_a is the partial pressure of atmospheric CO_2 (pCO_2); and C_s is the partial pressure of soil CO_2.

This relationship outlined in Equation 1 is commonly used to estimate past atmospheric CO_2 from paleosol carbonate $\delta^{13}C$ (Ekart et al., 1999; Breecker et al., 2010), assuming that some constraint can be made of the amount of soil-respired CO_2 (C_s; Montañez, 2013; Breecker and Retallack, 2014). Paleosol carbonate $\delta^{13}C$ has also been used to track changes in the distribution of C_3 versus C_4 vegetation (Quade et al., 1989; Latorre et al., 1997; Fox and Koch, 2003), as these vegetation types use different photosynthetic pathways that result in substantially different $\delta^{13}C$ values in plant matter (Farquhar et al., 1989; Edwards et al., 2010). Such work takes advantage of the fact that changes in δ_o causes changes in δ_s. Lastly, recent work has taken advantage of increasingly precise estimates of past atmospheric CO_2 (Cenozoic CO2 Proxy Integration Project Consortium et al., 2023) to estimate the soil CO_2 respiration flux, which directly influences the partial pressure of soil-respired CO_2 (Caves et al., 2016a; Rugenstein and Chamberlain, 2018; Licht et al., 2020). Soil respiration (ϕ_s) is linked to C_s via a 1-D production–diffusion equation first derived by Cerling (1984; Equation 2).

$$C_s = \frac{\phi_s \dot{z}^2}{D_s \varepsilon}\left(1 - e^{-\frac{z}{\dot{z}}}\right) \quad (2),$$

where D_s is the diffusion coefficient of CO_2 in soil, $\dot{z}$ is the characteristic decay depth of soil respiration, z is the depth in the soil of carbonate formation, and C_s is normalized to the soil porosity (ε) following Bowen and Beerling (2004). Equation 2 assumes that soil respiration decays exponentially with depth (Cerling and Quade, 1993). Because soil respiration—on timescales longer than the turnover time of organic carbon in the soil—is directly linked to aboveground plant productivity (Raich and Schlesinger, 1992), this method can be used to reconstruct landscape-scale plant productivity.

METHODS

Stratigraphic Sections

We sampled authigenic carbonates from five measured stratigraphic sections in the Albuquerque Basin (Fig. 1). Three sections (Arroyo Benavidez Sections 1 and 2 [AB1 and AB2] and the Southern Boulevard [SB] Section) approximately follow stratigraphic sections measured by Tedford and Barghoorn (1999), which allows us to tie our sections to their correlations to the Geomagnetic Polarity Timescale. These three sections include stratigraphic intervals in the Santa Fe Group that correspond to the Piedra Parada, Chamisa Mesa, and Cañada Pilares Members of the Zia Formation (~20 Ma–17.0 Ma) and the lower to middle part of the Cerro Conejo Formation (~14.8–12 Ma; Fig. 2). Note that an ~2-My-long unconformity (or possibly a tightly spaced series of disconformities coupled with a compressed section) is present in the lower Cerro Conejo Formation that separates ~17-Ma strata from ~14.8–12-Ma strata. In the following, we refer to this stratigraphic feature simply as the "lower Cerro Conejo unconformity." Koning et al. (in press) describes these sections, the age constraints, and the depositional environments. Note that the SB section is not a complete section of the Cerro Conejo Formation. Samples in the Piedra Parada Member (n = 4) and in the lower Chamisa Mesa Member (n = 4) were collected in 2019 and were measured only approximately relative to the base of the AB1 section.

We also measured two upper Miocene and early Pliocene stratigraphic sections (the Southeast Zia [SEZ] section and

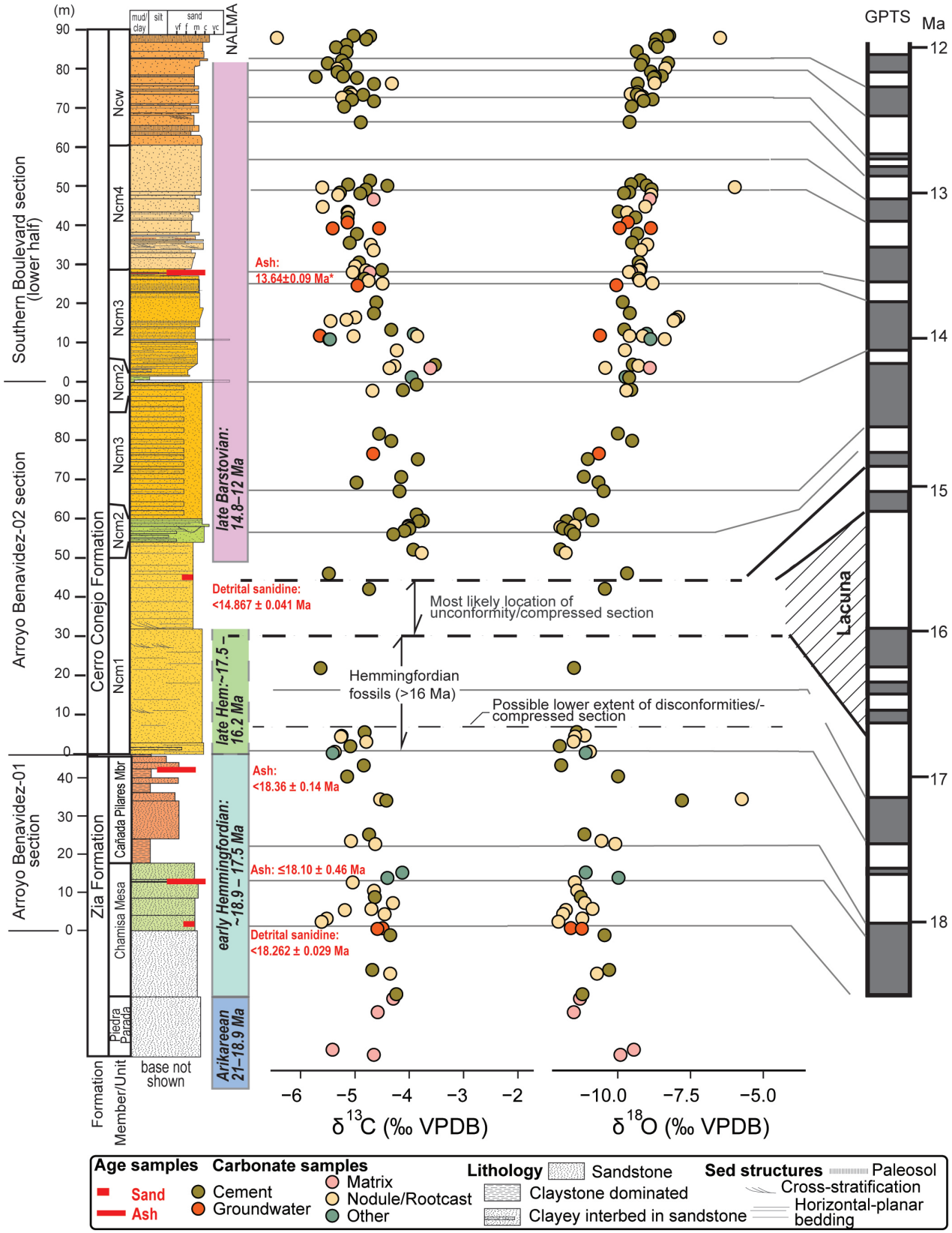


FIGURE 2. Stratigraphic section of the AB1, AB2, and SB sections (from Koning et al., in press). Authigenic carbonate $\delta^{13}C$ and $\delta^{18}O$ (‰ relative to the Vienna Pee Dee belemnite [VPDB] standard) are shown in the middle. Point color corresponds to the type of authigenic carbonate: brown is cement; reddish orange is groundwater; pink is matrix; tan is nodule or rootcast/rhizolith; green represents all other types of carbonates. Gray lines indicate correlations based upon detrital sanidine, tephra, and paleomagnetic measurements (Tedford and Barghoorn, 1999) to the Geomagnetic Polarity Timescale (GPTS). The approximate position of the unconformity in the Cerro Conejo is denoted by cross-hatching. Note that the base of the Chamisa Mesa Member is approximate and the base of the Piedra Parada Member is not shown. The tephra at 13.64 Ma is from Tedford and Barghoorn (1999). Unit designations from Koning et al. (in press).

the Southeast Zia Extension [SEZ-ext] section) within the Zia Pueblo (Fig. 3). In addition, we collected samples for organic carbon $\delta^{13}C$ analysis from the SEZ section. The SEZ-ext section ends at the escarpment that comprises the Llano del Albuquerque and at a regionally extensive petrocalcic horizon corresponding to the Rincones paleosurface (Connell, 2008).

In both sections, we sampled a variety of authigenic carbonate types, including nodules, rhizoliths and root casts, and cemented Bk horizons (labeled "matrix"). Samples were selected in the field using dilute (10%) hydrochloric acid (HCl) to test for the presence of carbonate and categorized by both the morphology of the sample and the depositional environment. All of these carbonates are thought to have formed in the vadose zone during ancient pedogenesis, and therefore the $\delta^{18}O$ should reflect paleometeoric water and the $\delta^{13}C$ should reflect the processes that influence paleo-soil pCO_2. We also sampled carbonate-cemented sandstones, using dilute (10%) HCl to affirm the presence of carbonate. Cementation in such rocks is thought to have occurred via shallow groundwater flow (Beckner and Mozley, 1998) shortly after deposition (labeled "cement" or "groundwater" if fluting was observed). Although these groundwater carbonates form from CO_2 dissolved within groundwater, ultimately that CO_2 is sourced from the vadose zone, and previous work has shown that carbonate-cemented sandstones have $\delta^{18}O$ and $\delta^{13}C$ values similar to those of time-equivalent vadose zone carbonates (Quade and Roe, 1999), including within the Albuquerque Basin (Beckner and Mozley, 1998).

Geochronology

We use age control and stratigraphy presented in Koning et al. (in press) to build an age model for the AB1, AB2, and SB sections. To build an age model for the SEZ and SEZ-ext sections, we collected samples for $^{40}Ar/^{39}Ar$ analysis that included sandstone samples for detrital sanidine (DS) analysis and six basalt clasts at the base of the Picuda Peak Member. For DS, the potassium feldspar (K-feldspar) portion of each sample was concentrated using heavy liquid separation, and sanidine crystals were handpicked in wintergreen oil under a polarizing transmitted light microscope (Heizler et al., 2021). Basalt clasts were crushed, ultrasonically treated in dilute HCl, and then rinsed extensively in distilled water while in an ultrasonic bath. Approximately 1-mm-diameter basalt fragments that were visibly free of phenocrysts and alteration were handpicked while being viewed under a binocular microscope. DS and basalt samples were irradiated in two batches, with batch NM-334 at the U.S. Geological Survey reactor in Denver, Colorado, and batch NM-345 at the Oregon State University reactor in Corvallis, Oregon, along with Fish Canyon Tuff sanidine (FC-2) as the neutron flux monitor. FC-2 is assigned an age of 28.201 Ma (Kuiper et al., 2008), and all dates were calculated with a total ^{40}K decay constant of $5.463 \times 10^{-10}/a$ (Min et al., 2000). All samples were analyzed at the New Mexico Geochronology Research Laboratory, Socorro, New Mexico. Argon isotopes extracted from the DS and FC-2 crystals were measured with an ARGUS VI mass spectrometer, whereas the basalt groundmass samples were analyzed with a Helix MC mass spectrometer. All dates are reported with $\pm 1\sigma$ analytical uncertainties that include the measurement of the neutron flux monitor uncertainty (J-factor). Complete analytical data and methods are given in Appendix 2.

Stable Isotopes

Carbonate stable isotopes

All carbonate samples were powdered by hand using either a Dremel or a mortar and pestle. We analyzed our samples at the Natural Resource Ecology Laboratory's (NREL) EcoCore Facility at Colorado State University (CSU), Fort Collins, Colorado, and we rejected samples that had less than 10% $CaCO_3$ content. Thus, depending upon carbonate content, we weighed between 207 and 1,875 µg of powdered sample. We placed these aliquots in 12-ml Exetainer vials, which were flushed with helium and then reacted with 99.99% phosphoric acid for 70 min at 70°C. Samples were analyzed for $\delta^{18}O$ and $\delta^{13}C$ using a Thermo-Fisher Delta V Advantage continuous-flow isotope-ratio mass spectrometer attached to a Thermo GasBench II. Repeat analysis of standards yields a standard deviation of less than 0.2‰ for $\delta^{18}O$ and less than 0.1‰ for $\delta^{13}C$.

Organic carbon stable isotopes

Aliquots of the samples selected for carbonate stable-isotope analysis were used to analyze for organic carbon $\delta^{13}C$. Samples (10–50 mg) were weighed, loaded into silver capsules, and fumigated in HCl for 6 hours to remove any carbonate, following the procedure in Harris et al. (2001). These aliquots were then oven dried and loaded into a Costech ECS 4010 elemental analyzer coupled to a Thermo-Fisher Delta V Advantage continuous-flow isotope-ratio mass spectrometer at the NREL EcoCore Facility at CSU. Repeat analysis of our glycine standard yielded a standard deviation of less than 0.2‰ for $\delta^{13}C$.

RESULTS

Stratigraphy

Arroyo Benavidez and Southern Boulevard sections

We sampled authigenic carbonate from well-exposed strata on the Ceja del Rio Puerco (Fig. 2; Koning et al., in press). The lithologic units include the Piedra Parada, Chamisa Mesa, and Cañada Pilares Members of the Zia Formation and the lower through middle Cerro Conejo Formation. Except for the claystone-rich Cañada Pilares Member, these strata are composed of mainly fine- to medium-grained sandstone. The Piedra Parada Member is a medium-grained eolianite, and the clayey Cañada Pilares Member is associated with a playa lake or broad floodplain. The rest of the strata are mainly tabular-bedded strata associated with deposition on the distal parts of broad fans or drainages (probably ephemeral) in distributive fluvial systems (Harley et al., 2010; Weissman et al., 2010). Details regarding

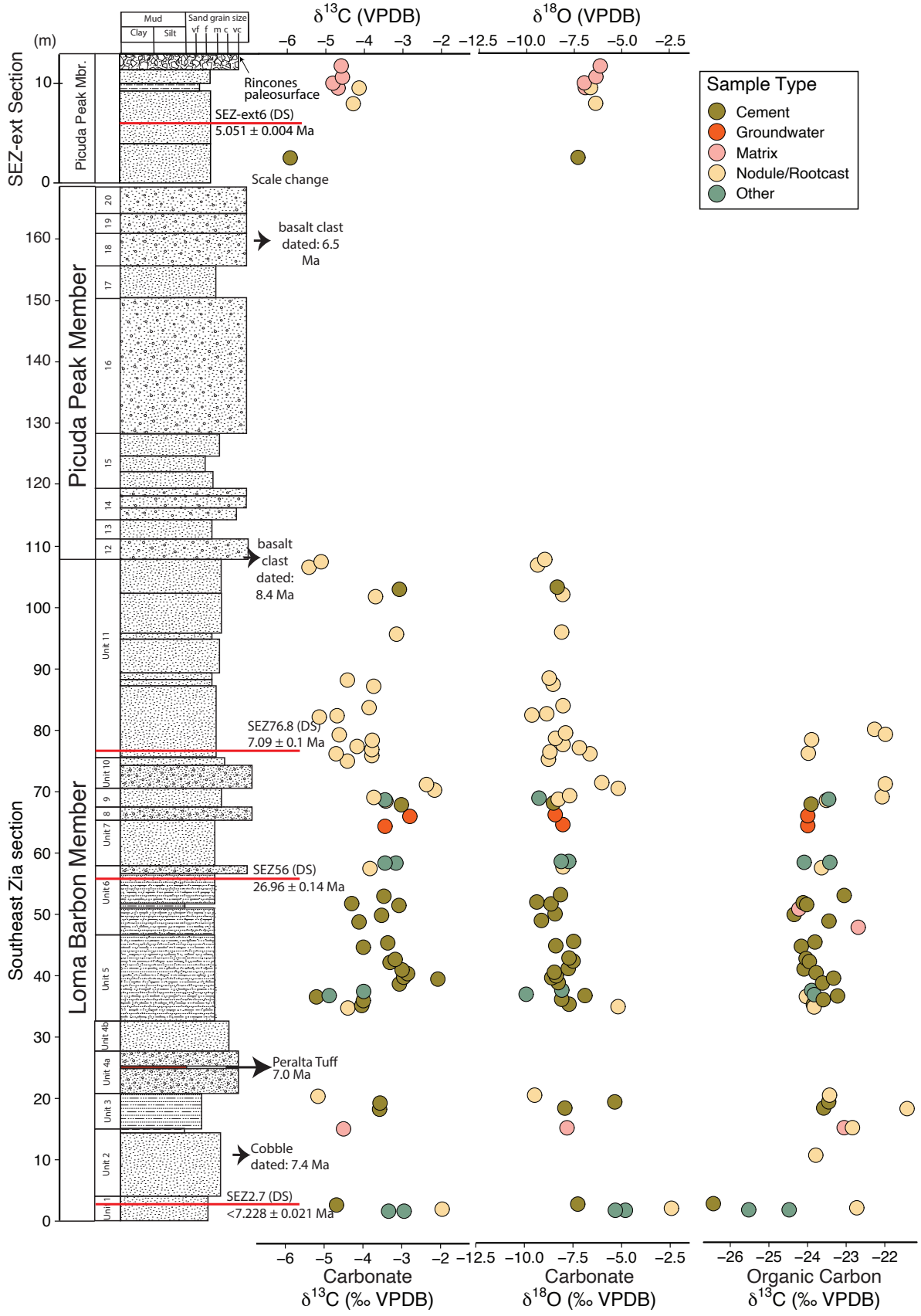


FIGURE 3. Stratigraphic section of the SEZ and SEZ-ext sections. Authigenic carbonate $\delta^{13}C$ and $\delta^{18}O$ and organic carbon $\delta^{13}C$ (‰ VPDB) are shown to the right. The age of the Peralta Tuff is from tephrochronology (Koning and Personius, 2002; Connell, 2008) and the ages of the 7.4-Ma cobble and the 6.5-Ma basalt cobble are from Koning and Personius (2002) and Connell (2008). Point color corresponds to the type of authigenic carbonate: brown is cement; reddish orange is groundwater; pink is matrix; tan is nodule or rootcast/rhizolith; green represents all other types of carbonates. Note the scale change between the SEZ and SEZ-ext section.

the lithologic character and depositional environments of these units are in Koning et al. (in press).

Southeast Zia section

The 167-m (548-ft)-thick Southeast Zia stratigraphic section was measured in the upper part of the Arroyo Ojito Formation (Fig. 3); a full description of the section is provided in Appendix 1. Its lower 108 m corresponds to the Loma Barbon Member and its upper 59 m correlates to the conglomeratic Picuda Peak Member (Connell, 2008). Uppermost Picuda Peak Member strata (12.5 m thick) are described and measured in the Southeast Zia Extension stratigraphic section, giving a total thickness of 71.5 m for the Picuda Peak Member.

From 0 to 60 m (0 to 197 ft) in stratigraphic height from the base of the SEZ section, the Loma Barbon Member consists of interbedded sandstone and subordinate clayey strata (i.e., mudstone and clayey sandstone). Beds are thin to thick and tabular. Clayey intervals are commonly mixed with very fine to fine sand, and mudstones may contain thin sandstone interbeds. Conglomerate is measured at 20.8–27.3 m (68–90 ft), within which is a ~1-m (~3-ft)-thick bed of fine white volcanic ash (23.5–24.6 m [77–81 ft]). This ash bed has been chemically correlated to the 7.0-Ma Peralta Tuff (Koning and Personius, 2002; Connell, 2008). From 65 to 76 m (213 to 249 ft), the sand is intercalated with minor conglomeratic tongues. Gravel is composed of granite, reworked Pedernal chert, intermediate volcanic rocks, and Permian–Triassic sandstones. Sand is light brown and fine to medium grained, and it has sparse paleosols characterized by cambic horizons underlain by weakly developed calcic horizons.

Sandstone dominates the upper Loma Barbon Member (76–108 m [249–354 ft] stratigraphic height). Associated bedding is medium to thick and tabular; within beds, sand is massive to horizontal-planar laminated. Sand is mainly fine to medium grained. Locally, up to 1% paleosol horizons are present that contain 1–3% $CaCO_3$ nodules.

The Picuda Peak Member consists of reddish, gravelly strata interbedded with 30% sand intervals. In the SEZ section, its base is a pronounced scoured surface that likely corresponds to a disconformity, as the general lithology is notably different above the contact. Sand occurs in 3–9-m-thick intervals and is mainly fine to coarse grained. Relatively weak consolidation results in poor exposure of bedding. Gravelly beds are tabular to lenticular and occur in 1–23-m (3–75-ft)-thick intervals. Gravel consists of pebbles with 5–15% cobbles. No obvious paleosols or authigenic calcium carbonate were noted in the sands. The uppermost 3 m of the Picuda Peak Member is a strongly developed, calcic paleosol. In the upper 1.2 m (4 ft) of the paleosol, there are signs of slight brecciation in the pedogenic cement, indicating a stage V carbonate morphology (Bachmann and Machette, 1977; Birkeland et al., 1991). Formation of such a well-developed soil would likely require a few to several hundreds of thousands of years of time (e.g., Machette, 1985) during which the surface was geomorphically stable. From this soil, four samples were collected, and two additional samples were collected 3.5 and 9 m (11 and 30 ft) below the top of the calcic soil.

Geochronology

Arroyo Benavidez and Southern Boulevard stratigraphic sections

New $^{40}Ar/^{39}Ar$ ages, synthesized with biostratigraphic and magnetostratigraphic data, allow well-constrained correlations with the Geomagnetic Polarity Time Scale (GPTS) for 18.5–17.2-Ma strata (upper Chamisa Mesa and Cañada Pilares Members of the Zia Formation and basal 5 m of strata in the Cerro Conejo Member). However, there is a cryptic unconformity in the lower Cerro Conejo Formation, and its stratigraphic position remains unclear. We follow Koning et al. (in press) in noting that this unconformity lies below a DS sample at 45 m (148 ft), dated to 14.867 Ma, and note that Tedford and Barghoorn (1999) suggest that fossils in the lowermost 30 m (98 ft) of the formation are best assigned to the Hemingfordian North American Land Mammal Age (17.5–16.2 Ma; Fig. 2). Thus, the unconformity is likely located between 30 and 45 meters (98 and 148 ft) in the AB2 section, but a zone of cryptic disconformities and a compressed section possibly could extend below 30 m (98 ft) to just above the well-exposed basal 5 m (16 ft) of the section. The unconformity could represent (1) a single true lacuna with a hiatus and a cryptic degradation vacuity (e.g., Wheeler, 1964); (2) a compressed section with multiple disconformities (degradational vacuities) plus sedimentation hiatuses; or (3) stacked hiatuses with no major erosional surfaces (no major degradational vacuity). The first option would most likely be present between 30 and 45 m (98–148 ft), whereas the other two could extend down to 5 m in the section. In Figure 4, we show how uncertainty regarding the position of this unconformity propagates through our age constraints on the AB1, AB2, and SB sections. Above the unconformity in the Cerro Conejo, a 13.64 ± 0.09-Ma volcanic ash (Tedford and Barghoorn, 1999) allows correlation to the GPTS that is well constrained for 14.8–13-Ma Cerro Conejo Formation. Specifically, we feel confident of the 14.1-Ma age for the green marker bed, which coincides with a change in general $\delta^{13}C$ values (below which values are higher). Correlations become less certain at distances >40 m (>131 ft) above this ash (>70 m [>230 ft] in the Southern Boulevard stratigraphic section), but it is likely that the youngest strata that we sampled are close to 12 Ma. See Koning et al. (in press) for details on the age control for these three stratigraphic sections.

SE Zia stratigraphic section

We present new $^{40}Ar/^{39}Ar$ data for four detrital sanidine (DS) samples and six basalt clasts in the upper Arroyo Ojito Formation (SEZ and SEZ-ext sections). Between 32 and 193 DS grains were dated; the dates are dispersed, with the majority being late Paleogene (Fig. 5; sheet 1 of Appendix 2). Sample SEZ-2.7 yields three grains of 121 total grains, giving a maximum depositional age (MDA) of 7.228 ± 0.021 Ma. Sample

SEZ-56 contains no Miocene grains, and the youngest grain is 26.96 ± 0.14 Ma. Sample SEZ-76.8 has a provisional MDA of 7.095 ± 0.096 Ma based on a single date from 120 total crystals. Lastly, sample SEZext-6.0 yields a robust MDA of 5.051 ± 0.004 Ma based on six dates from 193 total grains dated.

Unlike for the Arroyo Benavidez and Southern Boulevard stratigraphic sections, there has been no magnetostratigraphic work done near the SE Zia section. Given the Peralta Tuff age of 7.0 Ma at 24 m (79 ft) in the SE Zia section (Koning and Personius, 2002), the ages of the detrital sanidine samples in the SE Zia section are probably within 0.2 Ma of the true depositional ages. A minimum sedimentation rate of 125 m/My (25 m/0.2 My) is calculated using the Peralta Tuff age and a maximum depositional age of 7.2 Ma (sample SEZ-2.7). This rate is above the ~50 m/My average in the Ceja del Rio Puerco (Koning et al., in press) and slightly lower than the 150 m/My rate calculated using the Arroyo Ojito Formation below the Peralta Tuff (Connell et al., 2013). Using 125 m/My and 180 m/My as possible bounds on the sedimentation rate, the top of the Loma Barbon Member is about 6.5–6.3 Ma (Fig. 4B). In summary, our best estimate for the age of the carbonate samples in the Loma Barbon Member measured in the SEZ section is ~7.2 Ma through ~6.4 Ma (Fig. 4).

The unconformity-bounded Picuda Peak Member likely spans the latest Miocene through early Pliocene. Uppermost strata are younger than the maximum depositional age of 5.0 Ma, constrained by sample SEZext-6.0 m (20 ft; Figs. 3–5). A cobble from the upper middle of the Picuda Peak Member, 20 m (66 ft) below the upper contact, yielded a maximum depositional age of 6.5 Ma (Koning and Personius, 2002; Connell, 2008). Assuming that the unconformity associated with the lower contact is minor, the base of the Picuda Peak Member is likely close to 6 Ma. The basalt clast argon geochronology data are provided in Appendix 3. The six clast dates at

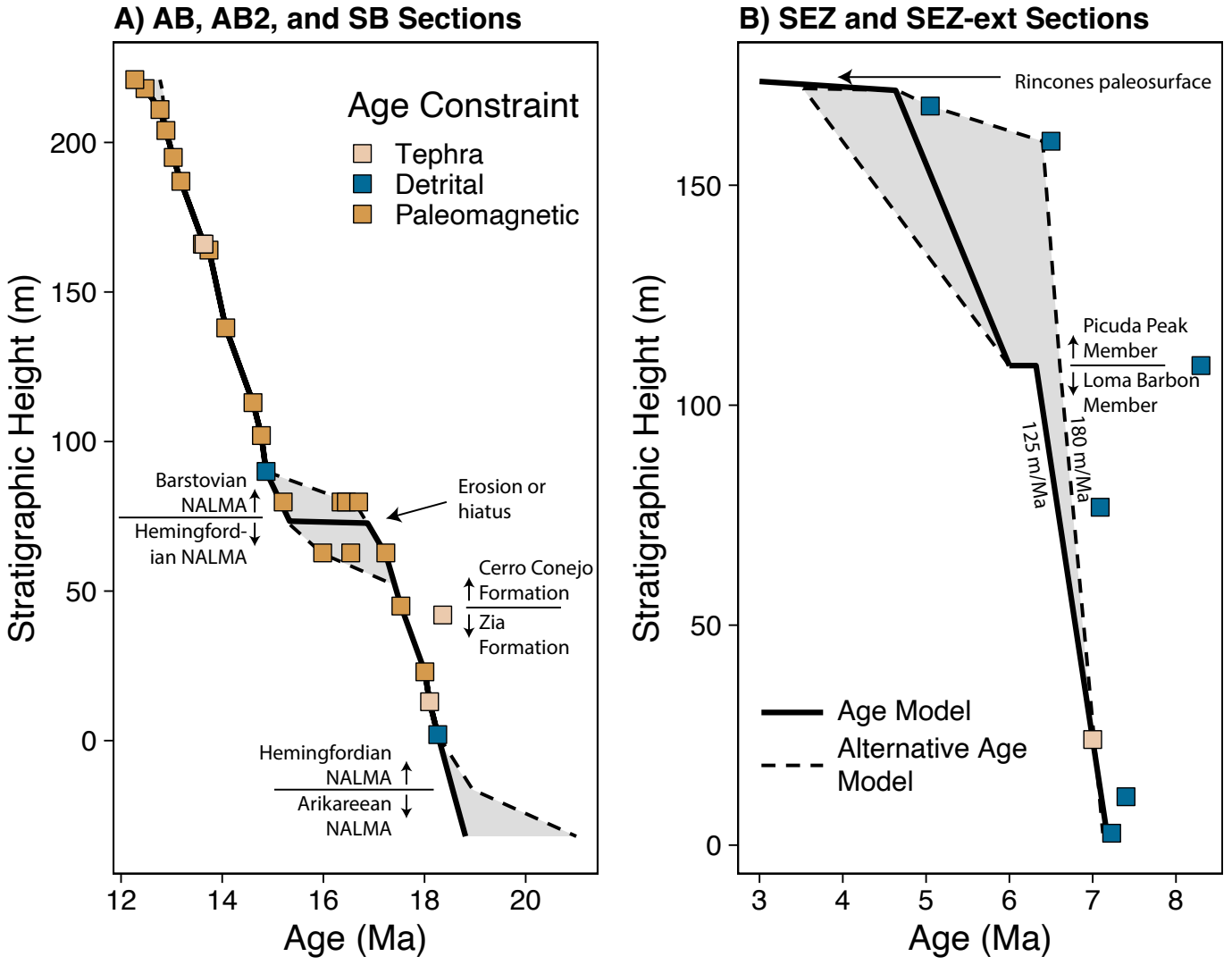


FIGURE 4. Age–thickness plots for A) the AB, AB2, and SB sections and B) the SEZ and SEZ-ext sections. Age constraints are shown as squares: tephra—either K/Ar, $^{40}Ar/^{39}Ar$, or tephrochronology—is tan; detrital constraints are blue; paleomagnetic constraints (Tedford and Barghoorn, 1999) are brown. Dashed lines show maximum and minimum age models; gray shading indicates that any age between the black lines is permissible given uncertainty in the age models. Solid black line shows the age model used to calculate the age of the authigenic carbonate samples.

the base of the Picuda Peak Member range between 8.400 ± 0.026 and 9.459 ± 0.015 Ma and do not further constrain the MDA derived from the 6.5-Ma cobble from the Picuda Peak Member. Deposition ceased sometime after 5 Ma, based upon our new 5.0-Ma DS maximum deposition age. Thus, calcium carbonate precipitation associated with formation of the capping, stage V petrocalcic soil (Rincones paleosurface) reflects local geomorphic stability during the early Pliocene, probably 5 through ~3 Ma. The ~3-Ma minimum age is consistent with the interpreted 4–3-Ma base of the younger Atrisco Member of the Ceja Formation (Connell et al., 2013), which to the south and southwest overlies the Rincones surface (Fig. 4). However, the time involved in soil formation could possibly be shorter (~1 My), so that the time of soil development could be 5–4 Ma or possibly 4–3 Ma.

Carbonate and Organic Carbon Stable Isotopes

We present 196 new authigenic carbonate stable-isotope values in Appendix 4. Overall, authigenic carbonate $\delta^{13}C$ averages −4.4 ± 0.8‰ (1σ), and the full range of values spans from −6.3 to −2.0‰. Average carbonate $\delta^{18}O$ is −9.0 ± 1.5‰ (1σ) with a full range of −11.6 to −2.4‰. There is an overall increasing trend in $\delta^{18}O$, whereas $\delta^{13}C$ increases and decreases throughout our sections (Figs. 2 and 3). There is a slight, but statistically significant, positive relationship between $\delta^{18}O$ and $\delta^{13}C$ (the slope of a linear regression between these two datasets has a p-value of <<0.05 and a 95% confidence interval >0; Fig. 6A). Though a number of types of carbonates are represented in these datasets, these different types of authigenic carbonates do not display different trends through time and do not have statistically significant differences in their $\delta^{13}C$ values (Figs. 2 and 3; Table 1). We do note that groundwater carbonates and carbonate cements have the lowest $\delta^{18}O$ values, whereas the lowest $\delta^{13}C$ values belong to authigenic carbonates that are thought to have formed within the vadose zone, including dispersed carbonate within paleosol matrices and rootcasts/rhizoliths, though these differences are not significant.

In the Piedra Parada, Chamisa Mesa, and Cañada Pilares Members, $\delta^{13}C$ averages −4.7 ± 0.5‰, with the lowest values toward the top of the Cañada Pilares Member. The Cerro Conejo Formation is characterized by low $\delta^{13}C$ values in the lower 45 m (148 ft) of the section, with a local maximum between 50 and 93 m (164–305 ft) and then declining $\delta^{13}C$ values upward in the Cerro Conejo (observed in the Southern Boulevard section; Fig. 2). Above the cryptic unconformity, $\delta^{13}C$ values are generally higher and slowly decrease upward in the Cerro Conejo Formation (Fig. 2). Intriguingly, one carbonate sample was collected at the same height as the DS sample that provides a maximum height for the unconformity, and this sample has relatively low $\delta^{13}C$, suggesting that the substantial increase in $\delta^{13}C$ observed at ~50 m (164 ft) in the Cerro Conejo Formation may be close but does not correspond exactly to the position of the unconformity.

When compared against global paleoclimate records, $\delta^{13}C$ is at its lowest in the late early Miocene, before the onset of the middle Miocene Climate Optimum (MCO; Fig. 7). Carbonate $\delta^{13}C$ has a local maximum at the 14.8–14.1 Ma during the Miocene Climate Transition (MCT). However, there are two carbonate samples with low $\delta^{13}C$ that may be located above the unconformity in the Cerro Conejo Formation (5–45 m [16–148 ft] in stratigraphic section AB2), placing them in the early middle Miocene, rather than in the late early Miocene before the onset of the MCO, as our preferred age model suggests (Fig. 4). Thus, we cannot robustly constrain the timing of the shift from low $\delta^{13}C$ to high $\delta^{13}C$ in the MCT. Notably, there is an overall 1.5‰ increase in paleosol carbonate $\delta^{13}C$ between the early to middle Miocene (except for 17–15 Ma) and the latest Miocene. However, there is a wider range of $\delta^{13}C$ values in the late Miocene than in the middle Miocene.

In the Loma Barbon Member (in our SEZ section), $\delta^{13}C$ is low from 0 to 40 m (0 to 131 ft, ~7.2 to ~6.9 Ma), then arguably higher at 40–72 m (131–236 ft; ~6.9 Ma through ~6.7 Ma using our estimated sedimentation rates), and then $\delta^{13}C$ becomes lower toward the top of the Loma Barbon Member (72–108 m [236–354 ft]; ~6.7 through ~6.4 Ma; Fig. 3). Lastly, the carbonates that comprise the early Pliocene petrocalcic horizon that caps the SEZ section (5–4 Ma) have $\delta^{13}C$ values that are, on average, slightly lower and less variable than those of the upper Loma Barbon Member. Except for the lowermost sample collected in the SEZ-extension section, all of these samples were obtained from above the DS sample dated at 5 Ma, indicating that these data lie firmly in the Pliocene. The

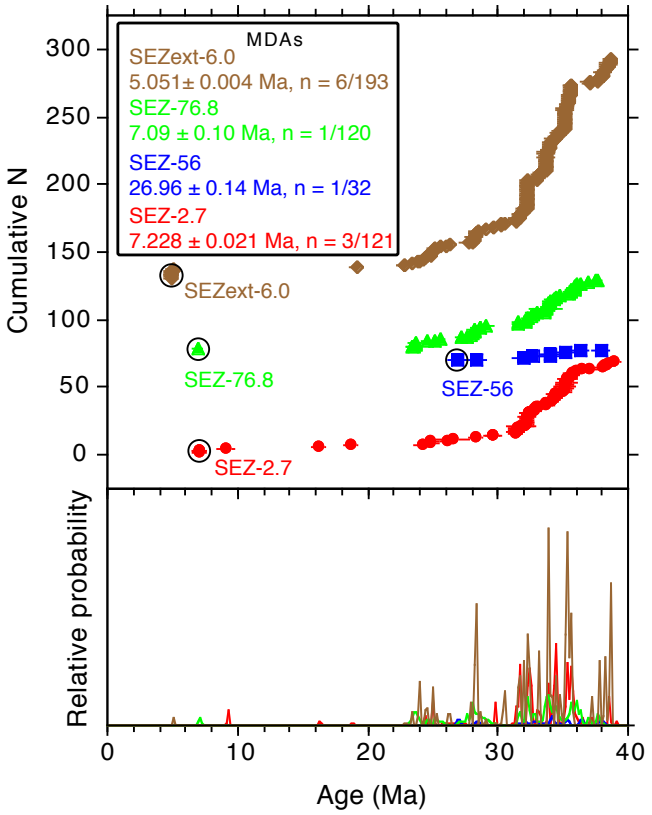


FIGURE 5. Relative probability and cumulative N diagrams for $^{40}Ar/^{39}Ar$ data from detrital sanidine in the SEZ and SEZ extension sections. MDA defining dates are outlined with open circle. Only dates younger than 40 Ma are presented; the complete dataset is provided in Appendix 2.

TABLE 1. Mean $\delta^{13}C$ and $\delta^{18}O$ (±1σ) associated with each authigenic carbonate sample type.

Carbonate type	Mean $\delta^{13}C$ (‰)	$\delta^{13}C$ 1σ (‰)	Mean $\delta^{18}O$ (‰)	$\delta^{18}O$ 1σ (‰)
Cement	−4.4	0.7	−9.2	1.2
Groundwater	−4.4	0.8	−9.6	1.0
Matrix	−4.6	0.4	−8.6	1.8
Nodule/rootcast/rhizolith	−4.5	0.8	−8.8	1.8
Other	−4.0	0.8	−8.5	1.8

petrocalcic horizon $\delta^{13}C$ values are slightly lower than that of a Holocene authigenic carbonate sampled from the deposits that overlie the Llano del Albuquerque geomorphic surface, though the $\delta^{18}O$ values are slightly higher in the petrocalcic horizon. We note that the exact timing of these trends is uncertain given the lack of robust age control in the SEZ and SEZ-ext sections; nevertheless, in bulk, these data clearly reflect the latest Miocene and early Pliocene.

In contrast to the complexity observed in the carbonate $\delta^{13}C$ data, carbonate $\delta^{18}O$ values generally increase through time, with the lowest values found in the Zia Formation during the late early Miocene and the trend continuing upward during the MCT and into the late Miocene (Fig. 7). The Pliocene petrocalcic horizon has some of the highest values, which are slightly higher than those for the same authigenic carbonate sampled from the Llano del Albuquerque surface.

Lastly, we measured 47 samples for organic carbon $\delta^{13}C$ data in the SEZ section (see Appendix 4). These data have a mean value of −23.6 ± 0.9‰ (1σ). There is no statistically significant relationship between the organic carbon $\delta^{13}C$ data and the authigenic carbonate $\delta^{13}C$ data (p-value of the slope of a linear regression between these two datasets is 0.43; Fig. 6B).

DISCUSSION

Our new data provide valuable insight into the evolution of paleoclimate and paleoenvironments in the Albuquerque Basin during the Miocene and builds upon earlier work by Beckner and Mozley (1998) that focused on $\delta^{18}O$ and $\delta^{13}C$ in the Zia and Cerro Conejo formations. Combined with new chronological constraints presented in Koning et al. (in press) and our new detrital sanidine $^{40}Ar/^{39}Ar$ ages from the Southeast Zia and Southeast Zia Extension sections, we can place our new stable-isotope data into a well-constrained stratigraphy. Though our age model for the SEZ and SEZ-ext sections is less well constrained than our age model for the AB1, AB2, and SB sections (Fig. 4), our isotope results are largely robust given the assumptions in our age model. Authigenic carbonate $\delta^{18}O$ has increased since the end of the MCO; authigenic carbonate $\delta^{13}C$ has also generally increased, with the highest values observed in the latest Miocene (i.e., within the SEZ section). In turn, the lowest $\delta^{13}C$ values appear in the early Miocene, before the onset of the MCO; however, these low values may have persisted past the end of the MCO, depending upon the timing and exact duration of the unconformity within the Cerro Conejo Formation.

Below, we discuss what implications these results hold for our understanding of past hydroclimate. We then discuss why our carbonate $\delta^{13}C$ record is best interpreted as a record of past productivity changes. Lastly, we place these interpretations in context with landscape-scale geomorphic and vegetation changes.

Neogene Hydroclimate Evolution

Carbonate $\delta^{18}O$ reflects precipitation $\delta^{18}O$ (Winnick et al., 2013; Manser et al., 2024), which in New Mexico is controlled by the seasonality of precipitation. The overall increase in carbonate $\delta^{18}O$ during the Miocene and into the Pliocene may reflect a shift in precipitation seasonality since the early Miocene. Comparably higher (−7 to −8‰) values are recorded for younger strata (13–12 Ma, 7.2–6.4 Ma, and 5–3 Ma) compared to earlier in the Miocene. Such a shift to greater summertime moisture might result from a combination of factors, including declining CO_2 over the Neogene (Cenozoic CO2 Proxy Integration Project Consortium et al., 2023), which in climate models configured with Miocene paleogeography results in a shift toward summertime precipitation (Acosta et al., 2024; Spaur et al., 2025). Furthermore, the opening in the late Miocene of the Gulf of California (cf. Chapin, 2008), which supplies approximately 50% of the moisture that reaches New Mexico during the North American Monsoon (Johnson and Delworth, 2022), may have resulted in elevated summertime precipitation. In contrast, paleosol carbonate $\delta^{18}O$ data from the high plains suggest that Gulf of Mexico moisture levels were approximately constant during the late Neogene (Manser et al., 2024). We note that, over this time period, the latitudinal position of the mid-latitude westerlies is likely to have shifted south in response to cooling (Abell et al., 2021), resulting in lower $\delta^{18}O$ (Gao et al., 2015); thus, the observed increase in $\delta^{18}O$ must reflect a change in seasonality that overwhelms this predicted global climate response.

Alternatively, the increase in carbonate $\delta^{18}O$ may reflect other or additional factors that operate on the fractionation between soil waters and carbonates, rather than on precipitation $\delta^{18}O$. For example, cooling over the course of the Neogene (Herbert et al., 2016), particularly in the northern hemisphere, would have had the effect of increasing carbonate $\delta^{18}O$ values if precipitation $\delta^{18}O$ remained constant, due to an increase in ^{18}O fractionation (Wostbrock et al., 2020). If aridity increased through the Miocene, increasingly evaporative conditions may have increased residual soil water $\delta^{18}O$, resulting in higher $\delta^{18}O$ values in the late Miocene and Pliocene (Kelson et al., 2023).

Indeed, the presence of petrocalcic paleosols suggests arid conditions that might enhance both landscape stability and the dust supply necessary to produce such a paleosol (Brock and Buck, 2009). Disentangling these factors will require additional geochemical work, such as clumped-isotope thermometry (Δ_{47}) measurements to estimate carbonate formation temperatures and $\delta^{17}O$ measurements to estimate any kinetic effects associated with authigenic carbonate formation (Rugenstein et al., 2022; Havranek et al., 2025).

Vegetation and Primary Productivity Changes

Carbonate $\delta^{13}C$ is thought to be influenced by atmospheric pCO_2, photosynthetic pathway (i.e., C_3 versus C_4 photosynthesis), and soil respiration (Cerling, 1984; Quade et al., 1989; Caves et al., 2016a). Over the course of our record, atmospheric pCO_2 declines, though the magnitude and timing of this decline remain uncertain (Fig. 7B; Cenozoic CO2 Proxy Integration Project Consortium et al., 2023). If atmospheric pCO_2 was the dominant driver of authigenic carbonate $\delta^{13}C$ in New Mexico, $\delta^{13}C$ values should decline between the middle and late Miocene. Though values do decline from ~14 to 12 Ma, $\delta^{13}C$ values rebound and reach higher values in the late Miocene. These trends suggest that the authigenic carbonates in the Albuquerque Basin may partially reflect atmospheric pCO_2 in the middle Miocene, but that other drivers overwhelm any atmospheric pCO_2 effect in the late Miocene.

Starting in the latest Miocene and continuing into the Pliocene, C_4 grasses colonized many grassland ecosystems, including those in North America (Fox and Koch, 2003). In the high plains, to the east of the Albuquerque Basin, C_4 grasses are thought to have comprised approximately 20% of the vegetation in the late Miocene and to have risen to dominance only in the Pliocene (Fox and Koch, 2003; Manser et al., 2024). To test whether the increase in carbonate $\delta^{13}C$ at 7.2–6.4 Ma, relative to the middle Miocene—and in particular the exceptionally high values (greater than −3‰) measured in the SEZ section—are a consequence of greater C_4 vegetation, we measured organic carbon $\delta^{13}C$ in samples collected between 0 and 80 m in the Loma Barbon Member in the Southeast Zia section (~7–6.6 Ma). These organic samples have relatively low $\delta^{13}C$ values. These low values are indicative of C_3 vegetation, particularly vegetation in arid localities (Kohn, 2010). In such locations, increased water use efficiency results in a smaller ^{13}C fractionation between atmospheric CO_2 and plant matter (Farquhar et al., 1989). A comparison with a published dataset of soil organic matter $\delta^{13}C$ from C_3 and C_4 landscapes (Montañez, 2013) indicates that the $\delta^{13}C$ values for our paleosol organic matter lie largely within the range of expected values for organic matter found in C_3 and C_3-dominant landscapes, but shifted slightly higher (Fig. 8). Further, five samples have relatively high organic carbon $\delta^{13}C$ (~22‰), which may reflect the influence of C_4 plants (Fig. 3). Even some mixed C_3–C_4 landscapes have low soil organic matter $\delta^{13}C$ (Fig. 8) due to the mixing of organic carbon from different plant types in soils, meaning that we cannot discount the possibility that some of the high carbonate and organic carbon $\delta^{13}C$ values reflect the presence of C_4 plants in the landscape. Such a possibility suggests that the late Miocene Albuquerque Basin landscape may have comprised a mosaic of different plants, perhaps predominantly C_3, but with a high enough abundance of C_4 plants to be locally recorded in soil carbonates. However, there is no

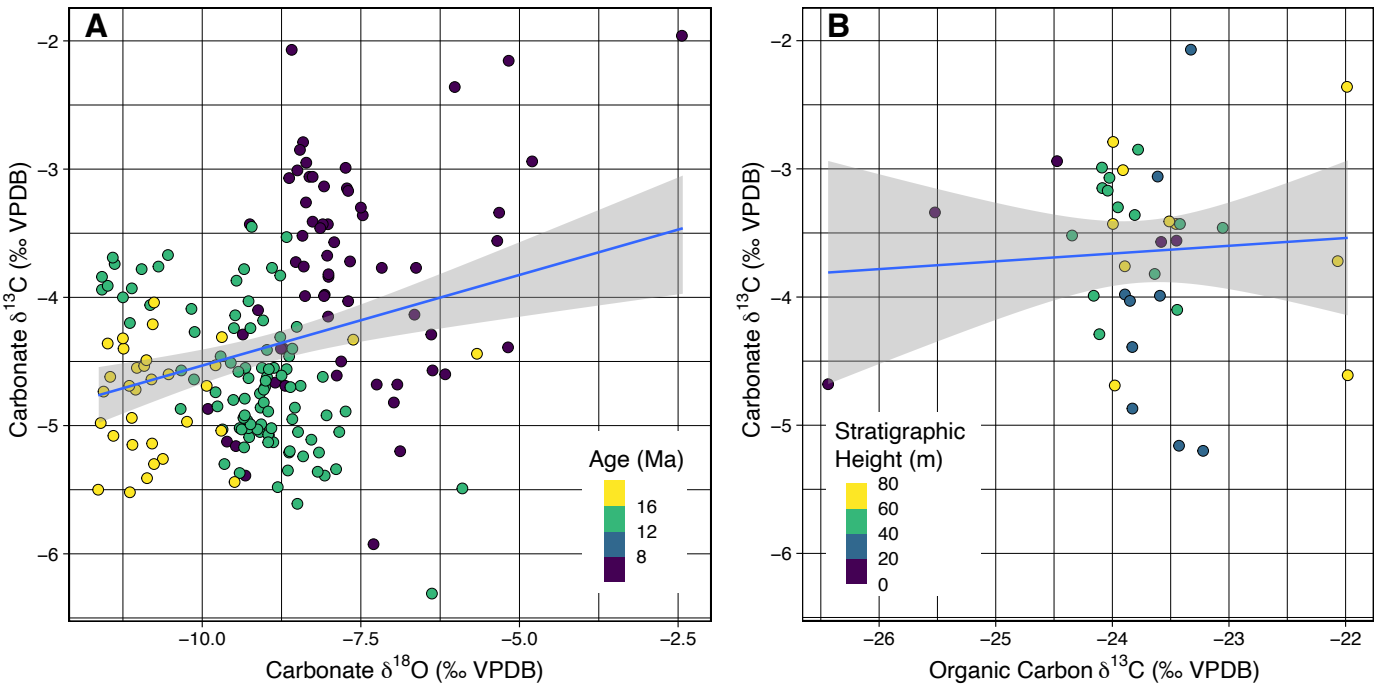


FIGURE 6. Cross-plots of carbonate $\delta^{13}C$ against carbonate $\delta^{18}O$ (A) and organic carbon $\delta^{13}C$ against carbonate $\delta^{13}C$ (B). The slope of the relationship in panel A is significant (p-value <<0.05), but there is no correlation in panel B (p-value of the slope of the linear regression is 0.43). Gray shading indicates the 95% confidence interval on the slope of the relationship.

statistically significant correlation between carbonate $\delta^{13}C$ and organic carbon $\delta^{13}C$, which may reflect different timescales of formation of soil carbonate (Havranek et al., 2025) relative to soil organic matter respiration. Thus, we conclude that the higher $\delta^{13}C$ values of the Loma Barbon member cannot be entirely explained by the appearance of C_4 plants in the Albuquerque Basin.

Instead, we suggest that some of the variation in authigenic carbonate $\delta^{13}C$ is due to changes in soil respiration related to changes in plant productivity. To estimate soil respiration, we use estimates of atmospheric pCO_2 from the Cenozoic CO_2 Proxy Intercomparison Project (Cenozoic CO2 Proxy Integration Project Consortium et al., 2023) to constrain the partial pressure of atmospheric CO_2, along with estimates of atmospheric CO_2 $\delta^{13}C$ from Tipple et al. (2010), and we assume that the mean value of organic matter $\delta^{13}C$ is constant throughout our record at −23.8‰. We detail the full set of parameters used in Equations 1 and 2 (above) and Table 2.

We present our estimates of soil respiration in Figure 7E. Each green point represents an estimate of soil respiration based on the corresponding carbonate $\delta^{13}C$ value and atmospheric pCO_2 interpolated to that age using the solid curve in Figure 7B. We find that soil respiration was highest in the late early Miocene. Unfortunately, the cryptic unconformity in the Cerro Conejo Formation precluded sedimentation during most of the MCO; consequently, we have no direct measurements of soil respiration during the peak warmth and high CO_2 of the MCO. During the MCT, soil respiration declined from 14.8 through 14.1 Ma and then was approximately constant from 14.1 through ~12 Ma. This constancy arises from the combination of declining carbonate $\delta^{13}C$ (Fig. 7D) and declining atmospheric CO_2 (Fig. 7B), which suggests that carbonate $\delta^{13}C$ in this part of the record may reflect changes in atmospheric CO_2. Soil respiration was on average lowest in the late Miocene (in the Southeast Zia section) and was slightly higher during the early Pliocene, as reflected by samples from the petrocalcic horizon that caps the SEZ-ext section.

We note that these soil respiration estimates are uncertain for a few reasons. First, the organic carbon $\delta^{13}C$ value for many of our samples are unknown as we possess data only for samples from the late Miocene Southeast Zia section. Second, atmospheric pCO_2 estimates are highly uncertain; however, paleoclimate and carbon cycle data indicate that it is likely that atmospheric CO_2 varied smoothly over the Neogene and did not rapidly change between low (<300 ppm) and high (>600 ppm) values (Caves et al., 2016b; Westerhold et al., 2020).

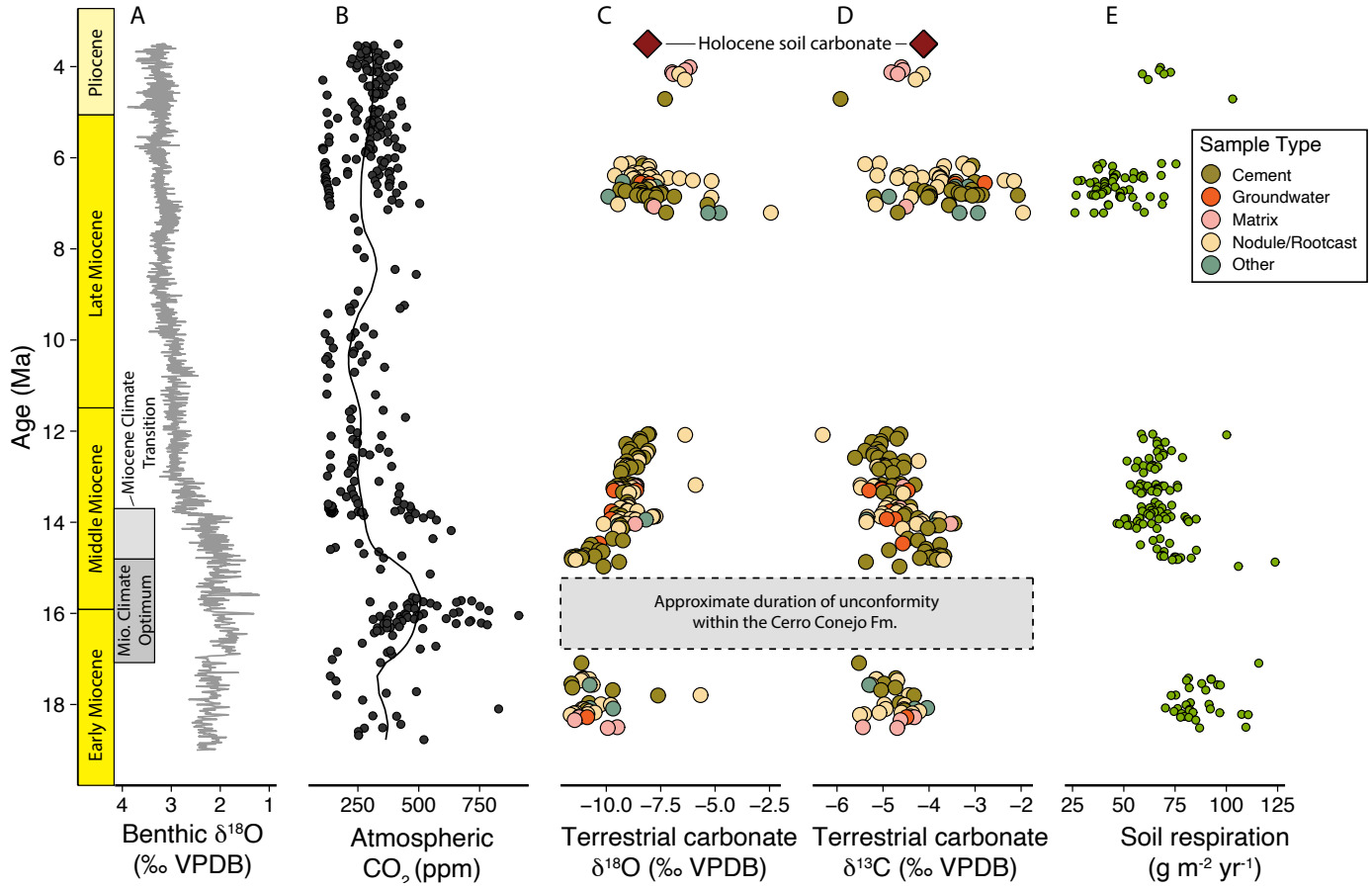


FIGURE 7. Albuquerque Basin paleoclimate records correlated to global records of Neogene climate. A) Benthic $\delta^{18}O$ (‰ VPDB) record of global climate (Westerhold et al., 2020). B) Atmospheric pCO_2 (ppm) proxy data (Cenozoic CO2 Proxy Integration Project Consortium et al., 2023). C) Authigenic carbonate $\delta^{18}O$ (‰ VPDB). D) Authigenic carbonate $\delta^{13}C$ (‰ VPDB). E) Estimated soil respiration (g m^{-2} yr^{-1}). The solid curve in panel B is a kernel-smooth average of paleoatmospheric CO_2 and this curve is used in our estimate of soil respiration (panel E).

Consequently, the effect of different atmospheric CO_2 estimates on our soil respiration estimates is to simply shift these estimates to higher (if atmospheric CO_2 is higher than the mean line in Fig. 7B) or lower (if atmospheric CO_2 is lower than the mean line in Fig. 7B) values, though the trend would stay largely steady over time scales of >1 Ma. We do note that our estimates of soil respiration suggest an approximate halving of soil respiration (and therefore plant productivity) between the early Miocene (19–17 Ma) and the latest Miocene (7.2–6.4 Ma).

Causes of Changing Soil Respiration and Plant Productivity

To a first-order, soil respiration is driven by aboveground plant productivity (Raich and Schlesinger, 1992). Plant productivity, particularly in mid-latitude environments, is closely linked to precipitation (Donohue et al., 2013; Yang et al., 2015). However, particularly in arid environments, it is also partly controlled by atmospheric CO_2. Atmospheric CO_2 is captured through stomata and converted to organic molecules within plant cells, and this process uses a tremendous amount of water (~500–1,000 g of water per gram of carbon) through a mechanism called transpiration. As atmospheric CO_2 rises, plants can fix a greater amount of carbon for the same amount of water. Because water is a limiting factor in arid environments, higher atmospheric CO_2 is thought to lead to greater leaf area and hence greater productivity (Donohue et al., 2013; Ukkola et al., 2016). Thus, the higher soil respiration during the early and middle Miocene may be at least partly driven by this CO_2 fertilization effect (20–17 Ma and 14.8–14.1 Ma strata in Fig. 7; Rugenstein and Chamberlain, 2018).

In New Mexico, the seasonality of precipitation may further impact plant productivity. Across the western United States, standing biomass is well correlated with the fraction of precipitation that is received in the winter (Kukla et al., 2022). We note that there is a slight positive correlation between carbonate $\delta^{18}O$ and $\delta^{13}C$ (Fig. 6A), although there are periods of our record (particularly in strata dated between 14.8 and 12 Ma) during which carbonate $\delta^{13}C$ and $\delta^{18}O$ are decoupled. Such decoupling may indicate that carbonate $\delta^{13}C$ was not linked to regional paleoenvironmental controls and instead reflects atmospheric pCO_2. Nevertheless, the overall positive correlation between authigenic carbonate $\delta^{18}O$ and $\delta^{13}C$ in our record (Fig. 6A) suggests that proportionately greater wintertime precipitation (i.e., low $\delta^{18}O$) results in greater plant productivity (i.e., low $\delta^{13}C$), whereas proportionately greater summertime precipitation (i.e., high $\delta^{18}O$) results in a more arid, less green landscape (i.e., high $\delta^{13}C$). A similar relationship was found by Spaur et al. (2025) during the middle Miocene in the Española Basin in northern New Mexico.

Consequences of Hydroclimate Changes on the Albuquerque Basin Landscape

Our new isotope records—and their paleoenvironmental interpretation—shed light on some of the stratigraphic changes that we observe in our sections. At the bottom of the Zia Formation, there is a shift from the predominantly eolian facies of the Piedra Parada Member to the basin floor/distal piedmont facies of the Chamisa Mesa Member (Fig. 2; Gawne, 1981; Koning et al., in press). The lack of a corresponding change in $\delta^{18}O$ and $\delta^{13}C$ values suggests that this shift was not climatically driven, but rather a response to a change in sand supply (Koning et al., in press). The overlying Cañada Pilares Member of the Zia Formation represents a broad floodplain or playa setting. Though the $\delta^{13}C$ there is not substantially different from the $\delta^{13}C$ values in the underlying Chamisa Mesa Member or the overlying lower Cerro Conejo Formation, some of the highest $\delta^{18}O$ values are within the Cañada Pilares, and these may reflect the role of evaporation in a playa or floodplain setting that causes higher $\delta^{18}O$ values.

The increasing shift toward summertime moisture after the end of the MCO is partly reflected in the stratigraphy. During 13–12 Ma, as carbonate $\delta^{18}O$ begins to increase, western piedmont facies prograde westward into the basin (Koning et al., in press). Although tectonic factors cannot be ruled out, this progradation could have been aided by a shift toward more intense, summertime convective storms (Koning et al., in press). The discharge associated with such storms could be expected to produce high overland flow discharges, facilitating erosion in upper paleodrainages and the transportation and deposition of the sediment on the western margin of the basin (e.g., Bull, 1991).

TABLE 2. Parameters used to calculate soil respiration from Albuquerque Basin carbonate $\delta^{13}C$, as shown in Figure 7E and Equations 1 and 2.

Parameter	Value	Units	Description	Source(s)
D_s	0.042	cm^2/s	Diffusional constant for CO_2 in soil	Cerling and Quade (1993)
ε	0.6	–	Porosity	Cerling and Quade (1993)
L	100	cm	Soil thickness	
z	50	cm	Depth of carbonate formation	Retallack (2005); Cerling and Quade (1993)
ż	25	cm	Characteristic decay depth of soil respiration	Cerling and Quade (1993)
δ_o	−23.8	‰	$\delta^{13}C$ of soil-respired organic matter	This study
T	25	°C	Temperature of carbonate formation	
δ_a	Variable	‰	Atmospheric CO_2 $\delta^{13}C$	Tipple et al. (2010)
C_a	Variable	‰	Atmospheric pCO_2	Cenozoic CO2 Proxy Integration Project Consortium et al. (2023)

Our estimates of changing plant productivity also hold implications for understanding the role of paleovegetation in supporting paleofaunas and in modifying landscape-scale water balance. One consequence of greater plant productivity in the late early and middle Miocene would have been a greener landscape, sustained by greater primary productivity. In the Española Basin during the MCO, a minimum in $\delta^{13}C$ and an estimated maximum in plant productivity correspond with a peak in mammalian diversity as preserved in the Santa Fe Group (Williamson and Sweet, 2024; Spaur et al., 2025). Is such a link between climate, productivity, and diversity evident in the Albuquerque Basin? Unfortunately, the unconformity in the Cerro Conejo Formation during the MCO in our section precludes an easy assessment of this question, and the mammalian fossil record is less well detailed than in the Española Basin. Nevertheless, the existing mammalian fossil record broadly supports greater faunal diversity during the middle Miocene compared to the late Miocene (Tedford and Barghoorn, 1999; Tedford et al., 2004), though this may reflect a lack of fossils in upper Miocene sediments (perhaps due to preservation factors) rather than an absolute change in diversity.

Lastly, greater plant productivity may not be related to greater water availability in the landscape, particularly if such an increase in productivity was driven primarily by CO_2 fertilization (Rugenstein and Chamberlain, 2018). In that case, greater productivity may have been sustained by efficient plant water use, limiting infiltration and resulting in reduced runoff (Mankin et al., 2017). Alternatively, greater productivity could be sustained by an increase in mean annual precipitation with no attendant change in how that precipitation is partitioned between plant water use and infiltration. Unfortunately, carbonate $\delta^{18}O$ alone does not directly provide information on changes in mean annual precipitation, given the myriad additional factors that modify carbonate $\delta^{18}O$. Although our data do indicate a shift in precipitation seasonality, that shift is observed in both groundwater and vadose-zone carbonate $\delta^{18}O$ (Figs. 2, 3, and 7). Consequently, how precipitation was partitioned between plant use and infiltration may not have changed through time, though the myriad factors that modify $\delta^{18}O$ may obscure such shifts. Additional work coupling newer proxy systems—such as $\delta^{17}O$ and Δ_{47} combined with detailed observations of sedimentary facies—may yield insight into the sensitivity of this partitioning through time as atmospheric CO_2 and vegetation change, and therefore into how southwestern hydroclimate may respond to rising atmospheric CO_2 and warming.

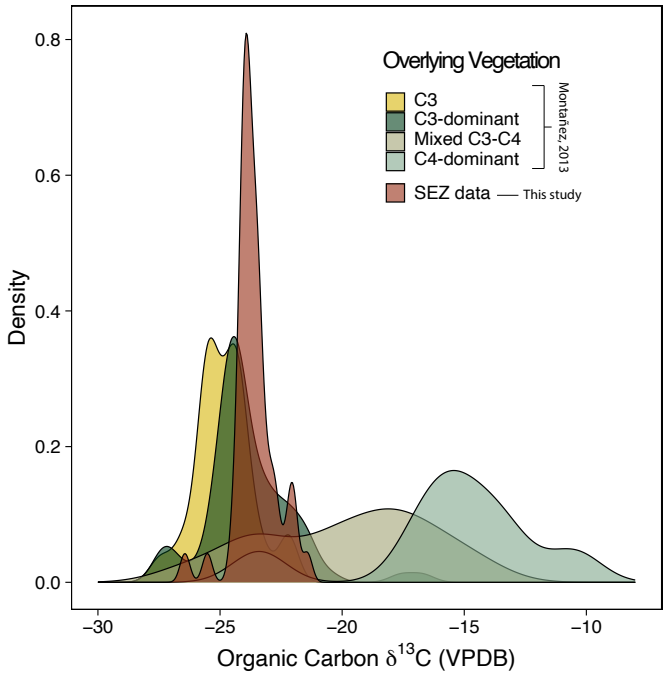


FIGURE 8. A density plot comparison between a compilation of soil organic carbon $\delta^{13}C$ from C_3, C_3-dominant, mixed C_3–C_4, and C_4-dominant landscapes from Montañez (2013) with our late Miocene paleosol organic matter $\delta^{13}C$ (red).

CONCLUSIONS

We present a new stable-isotope record from Miocene Santa Fe Group sediments in the Albuquerque Basin and combine this record with new sedimentology and geochronology work to tie our record to global records of paleoclimate. Our new geochronological constraints place the deposition of the upper part of the Loma Barbon Member of the Arroyo Ojito Formation between 7.2 Ma and ~6.4 Ma and the age of the Rincones paleosurface as younger than 5 Ma. Our new authigenic carbonate $\delta^{18}O$ record shows increases through time, suggesting a larger contribution of summertime moisture to annual precipitation in the latest Miocene compared to the late early and middle Miocene, likely driven by a combination of declining atmospheric CO_2 in the late Neogene and the opening of the Gulf of California, which provided abundant moisture to the North American Monsoon. The pattern for authigenic carbonate $\delta^{13}C$ is more complicated, with increases and decreases throughout the section. The overall increase in carbonate $\delta^{13}C$ between the early and middle Miocene and the late Miocene is likely due to a reduction in plant productivity, potentially tied to decreasing atmospheric CO_2 and declining wintertime moisture. Based upon new organic carbon $\delta^{13}C$ data from the late Miocene, we suggest that C_4 vegetation was not abundant and likely does not explain the majority of the increase in authigenic carbonate $\delta^{13}C$. Overall, this new record from the Albuquerque Basin is consistent with previous work from Santa Fe Group sediments in the Española Basin to the north suggesting that, during periods of higher atmospheric CO_2, northern and central New Mexico received a greater fraction of its annual moisture in the winter. Furthermore, the vegetation in the northwest Albuquerque Basin appears to have been more productive and likely resulted in a greener landscape during periods of higher atmospheric CO_2 (e.g., early Miocene), perhaps in response to CO_2 fertilization or to a higher proportion of wintertime precipitation. Disentangling how paleogeographic changes and global climate fluctuations may have driven these changes remains a pressing need in order to more accurately predict how climate and ecosystems will respond to ongoing anthropogenic warming.

ACKNOWLEDGMENTS

We thank the many individuals who assisted with field work, including Tyler Kukla, Katharina Methner, Thu Bui, Claire Pickerel, Clara Gilliam, Xueyao Cheng, and Gaby Sanchez Ortiz. We also thank Dan Reuss and EcoCore Analytical Services (RRID: SCR_011015) for assistance with sample measurements and the Santa Ana and Zia Pueblos for access to outcrops. We thank Daniel Breecker and Sean Connell for reviews that substantially improved this contribution. This project was funded by U.S. National Science Foundation (NSF) grant EAR-2202916 to J.K.C. Rugenstein, NSF grant FRES 2121594 to I.P. Montañez, and a mini-grant from the EcoCore Core Facility, Natural Resource Ecology Laboratory, Colorado State University.

REFERENCES

Abell, J.T., Winckler, G., Anderson, R.F., and Herbert, T.D., 2021, Poleward and weakened westerlies during Pliocene warmth: Nature, v. 589, p. 70–75. https://doi.org/10.1038/s41586-020-03062-1

Acosta, R.P., Burls, N.J., Pound, M.J., Bradshaw, C.D., De Boer, A.M., Herold, N., Huber, M., Liu, X., Donnadieu, Y., Farnsworth, A., Frigola, A., Lunt, D.J., von der Heydt, A.S., Hutchinson, D.K., Knorr, G., Lohmann, G., Marzocchi, A., Prange, M., Sarr, A.C., Li, X., and Zhang, Z., 2024, A model-data comparison of the hydrological response to Miocene warmth: Leveraging the MioMIP1 opportunistic multi-model ensemble: Paleoceanography and Paleoclimatology, v. 39, e2023PA004726. https://doi.org/10.1029/2023pa004726

Alessi, M.J., and Rugenstein, M., 2024, Potential near-term wetting of the southwestern United States if the Eastern and Central Pacific cooling trend reverses: Geophysical Research Letters, v. 51, p. e2024GL108292. https://doi.org/10.1029/2024GL108292

Asmerom, Y., Polyak, V.J., and Burns, S.J., 2010, Variable winter moisture in the southwestern United States linked to rapid glacial climate shifts: Nature Geoscience, v. 3, p. 114–117. https://doi.org/10.1038/ngeo754

Bachmann, G.O., and Machette, M.N., 1977, Calcic soils and calcretes in the southwestern United States: USGS Open-file Report, v. 77–794, 163 p. https://doi.org/10.3133/ofr77794

Beckner, J.R., and Mozley, P.S., 1998, Origin and spatial distribution of early vadose and phreatic calcite cements in the Zia Formation, Albuquerque Basin, New Mexico, USA, *in* Marod, S. ed., Carbonate Cementation in Sandstones: Distribution Patterns and Geochemical Evolution: Blackwell Publishing, v. 26, p. 27–51. https://doi.org/10.1002/9781444304893.ch2

Bernstein, R., Koning, D.J., Maloney, A., Spaur, S., Lee, O., Sanchez Ortiz, G., Methner, K., Mulch, A., Fiebig, J., Ibarra, D.E., Acosta, R.P., Snell, K.E., and Rugenstein, J.K.C., 2026, Neogene U.S. Southwest temperatures paced by global climate: European Geosciences 2026 General Assembly, Vienna, Austria, May 3–8, 2026, EGU26-14189. https://doi.org/10.5194/egusphere-egu26-14189

Bhattacharya, T., Feng, R., Tierney, J.E., Rubbelke, C., Burls, N., Knapp, S., and Fu, M., 2022, Expansion and intensification of the North American monsoon during the Pliocene: AGU Advances, v. 3, e2022AV000757. https://doi.org/10.1029/2022av000757

Birkeland, P., Machette, M.N., and Haller, K.M., 1991, Soils as a tool for applied Quaternary geology: Utah Geological and Mineral Survey, Miscellaneous Publication 91-3, 63 p.

Bowen, G.J., and Beerling, D.J., 2004, An integrated model for soil organic carbon and CO_2: Implications for paleosol carbonate pCO_2 paleobarometry: Global Biogeochemical Cycles, v. 18, GB1026. https://doi.org/10.1029/2003GB002117

Breecker, D.O., and Retallack, G.J., 2014, Refining the pedogenic carbonate atmospheric CO_2 proxy and application to Miocene CO_2: Palaeogeography, Palaeoclimatology, Palaeoecology, v. 406, p. 1–8. https://doi.org/10.1016/j.palaeo.2014.04.012

Breecker, D.O., Sharp, Z.D., and McFadden, L.D., 2010, Atmospheric CO_2 concentrations during ancient greenhouse climates were similar to those predicted for A.D. 2100: Proceedings of the National Academy of Sciences of the United States of America, v. 107, p. 576–580. https://doi.org/10.1073/pnas.0902323106

Brock, A.L., and Buck, B.J., 2009, Polygenetic development of the Mormon Mesa, NV petrocalcic horizons: Geomorphic and paleoenvironmental interpretations: Catena, v. 77, p. 65–75. https://doi.org/10.1016/j.catena.2008.12.008

Bull, W.B., 1991, Geomorphic Responses to Climatic Change: New York, NY, Oxford University Press, 326 p.

Caves, J.K., Sjostrom, D.J., Mix, H.T., Winnick, M.J., and Chamberlain, C.P., 2014, Aridification of Central Asia and uplift of the Altai and Hangay Mountains, Mongolia: Stable isotope evidence: American Journal of Science, v. 314, p. 1171–1201. https://doi.org/10.2475/08.2014.01

Caves, J.K., Moragne, D.Y., Ibarra, D.E., Bayshashov, B.U., Gao, Y., Jones, M.M., Zhamangara, A., Arzhannikova, A.V., Arzhannikov, S.G., and Chamberlain, C.P., 2016a, The Neogene de-greening of Central Asia: Geology, v. 44, p. 887–890. https://doi.org/10.1130/G38267.1

Caves, J.K., Jost, A.B., Lau, K.V., and Maher, K., 2016b, Cenozoic carbon cycle imbalances and a variable silicate weathering feedback: Earth and Planetary Science Letters, v. 450, p. 152–163. https://doi.org/10.1016/j.epsl.2016.06.035

Cenozoic CO2 Proxy Integration Project (CenCO2PIP) Consortium, Hönisch, B., Royer, D.L,. Breecker, D.O., Polissar, P.J., Bowen, G.J., Henehan, M.J., Cui, Y., Steinthorsdottir, M., McElwain, J.C., Kohn, M.J., Pearson, A., Phelps, S.R., Uno, K.T., Ridgwell, A., Anagnostou, E., Austermann, J., Badger, M.P.S., Barclay, R.S., Bijl, P.K., Chalk, T.B., Scotese, C.R., de la Vega, E., DeConto, R.M., Dyez, K.A., Ferrini, V., Franks, P.J., Giulivi, C.F., Gutjahr, M., Harper, D.T., Haynes, L.L., Huber, M., Snell, K.E., Keisling, B.A., Konrad, W., Lowenstein, T.K., Malinverno, A., Guillermic, M., Mejía, L.M., Milligan, J.N., Morton, J.J., Nordt, L., Whiteford, R., Roth-Nebelsick, A., Rugenstein, J.K.C., Schaller, M.F., Sheldon, N.D., Sosdian, S., Wilkes, E.B., Witkowski, C.R., Zhang, Y.G., Anderson, L., Beerling, D.J., Bolton, C., Cerling, T.E., Cotton, J.M., Da, J., Ekart, D.D., Foster, G.L., Greenwood, D.R., Hyland, E.G., Jagniecki, E.A., Jasper, J.P., Kowalczyk, J.B., Kunzmann, L., Kürschner, W.M., Lawrence, C.E., Lear, C.H., Martínez-Botí, M.A., Maxbauer, D.P., Montagna, P., Naafs, B.D.A., Rae, J.W.B., Raitzsch, M., Retallack, G.J., Ring, S.J., Seki, O., Sepúlveda, J., Sinha, A., Tesfamichael, T.F., Tripati, A., van der Burgh, J., Yu, J., Zachos, J.C., and Zhang, L., 2023, Toward a Cenozoic history of atmospheric CO_2: Science, v. 382, eadi5177. https://doi.org/10.1126/science.adi5177

Cerling, T.E., 1984, The stable isotopic composition of modern soil carbonate and its relationship to climate: Earth and Planetary Science Letters, v. 71, p. 229–240. https://doi.org/10.1016/0012-821X(84)90089-X

Cerling, T.E., 1999, Stable carbon isotopes in palaeosol carbonates, *in* Thiry, M., and Simon-Coinçon, R. eds., Palaeoweathering, Palaeosurfaces and Related Continental Deposits: International Association of Sedimentologists, p. 43–60. https://doi.org/10.1002/9781444304190.ch2

Cerling, T.E., and Quade, J., 1993, Stable carbon and oxygen isotopes in soil carbonates, *in* Swart, P.K., Lohmann, K.C., McKenzie, J., and Savin, S. eds., Climate Change in Continental Isotopic Records: American Geophysical Union, p. 217–231. https://doi.org/10.1029/GM078p0217

Chapin, C.E., 2008, Interplay of oceanographic and paleoclimate events with tectonism during middle to late Miocene sedimentation across the southwestern USA: Geosphere, v. 4, p. 976–991. https://doi.org/10.1130/GES00171.1

Connell, S.D., 2008, Refinements to the stratigraphic nomenclature of the Santa Fe Group, northwestern Albuquerque Basin, New Mexico: New Mexico Geology, v. 31, p. 14–35. https://doi.org/10.58799/NMG-v30n1.14

Connell, S.D., Smith, G.A., Geissman, J.W., and McIntosh, W.C., 2013, Climatic controls on nonmarine depositional sequences in the Albuquerque Basin, Rio Grande rift, north-central New Mexico: Geological Society of America Special Papers, v. 494, p. 383–425. https://doi.org/10.1130/2013.2494(15)

Dominguez, F., Miguez-Macho, G., and Hu, H., 2016, WRF with water vapor tracers: A study of moisture sources for the North American Monsoon: Journal of Hydrometeorology, v. 17, p. 1915–1927. https://doi.org/10.1175/JHM-D-15-0221.1

Donohue, R.J., Roderick, M.L., McVicar, T.R., and Farquhar, G.D., 2013, Impact of CO_2 fertilization on maximum foliage cover across the globe's warm, arid environments: Geophysical Research Letters, v. 40, p. 3031–3035. https://doi.org/10.1002/grl.50563

Edwards, E.J., Osborne, C.P., Strömberg, C.A.E., Smith, S.A., and Consortium, C.G., 2010, The origins of C_4 grasslands: Integrating evolutionary and ecosystem science: Science, v. 328, p. 587–591. https://doi.org/10.1126/science.1177216

Ekart, D.D., Cerling, T.E., Montañez, I.P., and Tabor, N.J., 1999, A 400 million year carbon isotope record of pedogenic carbonate: Implications for paleoatmospheric carbon dioxide: American Journal of Science, v. 299, p. 805–827. https://doi.org/10.2475/ajs.299.10.805

Farquhar, G.D., Ehleringer, J.R., and Hubick, K.T., 1989, Carbon isotope discrimination and photosynthesis: Annual Review of Plant Physiology and Plant Molecular Biology, v. 40, p. 503–537. https://doi.org/10.1146/annurev.pp.40.060189.002443

Fox, D.L., and Koch, P.L., 2003, Tertiary history of C_4 biomass in the Great Plains, USA: Geology, v. 31, p. 809–812. https://doi.org/10.1130/G19580.1

Gao, Y., Ibarra, D.E., Wang, C., Caves, J.K., Chamberlain, C.P., Graham, S.A., and Wu, H., 2015, Mid-latitude terrestrial climate of East Asia linked to global climate in the Late Cretaceous: Geology, v. 43, p. 287–290. https://doi.org/10.1130/G36427.1

Gawne, C.E., 1981, Sedimentology and stratigraphy of the Miocene Zia sand of New Mexico: GSA Bulletin, v. 92, p. 2484–2552. https://doi.org/10.1130/GSAB-P2-92-2484

Harris, D., Horwáth, W.R., and Van Kessel, C., 2001, Acid fumigation of soils to remove carbonates prior to total organic carbon or CARBON-13 isotopic analysis: Soil Science Society of America Journal, v. 65, p. 1853–1856. https://doi.org/10.2136/sssaj2001.1853

Havranek, R., Snell, K., Brookins, S., and Davidheiser-Kroll, B., 2025, Timing of pedogenic carbonate formation in fine-grained soils: Decoupled $T(\Delta_{47})$ and $\delta^{18}O_w$ seasonal bias: Paleoceanography and Paleoclimatology, v. 40, p. e2024PA005071. https://doi.org/10.1029/2024PA005071

Heizler, M.T., Karlstrom, K.E., Albonico, M., Hereford, R., Beard, L.S., Cather, S.M., Crossey, L.J., and Sundell, K.E., 2021, Detrital sanidine $^{40}Ar/^{39}Ar$ dating confirms <2 Ma age of Crooked Ridge paleoriver and subsequent deep denudation of the southwestern Colorado Plateau: Geosphere, v. 17, p. 438–454. https://doi.org/10.1130/GES02319.1

Herbert, T.D., Lawrence, K.T., Tzanova, A., Peterson, L.C., Caballero-Gill, R., and Kelly, C.S., 2016, Late Miocene global cooling and the rise of modern ecosystems: Nature Geoscience, v. 9, p. 843–847. https://doi.org/10.1038/ngeo2813

Hu, H., and Dominguez, F., 2015, Evaluation of oceanic and terrestrial sources of moisture for the North American monsoon using numerical models and precipitation stable isotopes: Journal of Hydrometeorology, v. 16, p. 19–35. https://doi.org/10.1175/JHM-D-14-0073.1

Jochems, A.P., and Morgan, G.S., 2018, A stable isotope record from paleosol and groundwater carbonate of the Plio-Pleistocene Camp Rice Formation, Hatch-Rincon Basin, southern New Mexico: New Mexico Geological Society, Guidebook 69, p. 109–117. https://doi.org/10.56577/FFC-69.109

Johnson, B.O., and Delworth, T.L., 2022, The role of the Gulf of California in the North American monsoon: Journal of Climate, v. 36, p. 1541–1559. https://doi.org/10.1175/jcli-d-22-0365.1

Kelson, J.R., Huth, T.E., Passey, B.H., Levin, N.E., Peterwen, S.V., Ballato, P., Beverly, E.J., Breecker, D.O., Hake, G.D., Hudson, A.M., Ji, H., Licht, A., Oerter, E.J., and Quade, J., 2023, Triple oxygen isotope compositions of globally distributed soil carbonates record widespread evaporation of soil waters: Geochimica et Cosmochimica Acta, v. 355, p. 138–160. https://doi.org/10.1016/j.gca.2023.06.034

Kohn, M.J., 2010, Carbon isotope compositions of terrestrial C_3 plants as indicators of (paleo)ecology and (paleo)climate: Proceedings of the National Academy of Sciences of the United States of America, v. 107, p. 19,691–19,695. https://doi.org/10.1073/pnas.1004933107

Koning, D.J., and Personius, S.F., 2002, Geologic map of the Bernalillo NW Quadrangle, Sandoval County, New Mexico: United States Geological Survey, Miscellaneous Field Studies Map 2404, scale 1:24,000. https://doi.org/10.3133/mf2404

Koning, D.J., Ricci, J., Connell, S.D., Rugenstein, J.K.C., and Morgan, G.S., in press, Stratigraphy, paleoenvironments, and depositional controls of the lower–middle Santa Fe Group along the Ceja del Puerco, northwestern Albuquerque Basin, New Mexico: New Mexico Geology.

Kuiper, K.F., Deino, A., Hilgen, F.J., Krijgsman, W., Renne, P.R., and Wijbrans, J.R., 2008, Synchronizing rock clocks of Earth history: Science, v. 320, p. 500–504. https://doi.org/10.1126/science.1154339

Kukla, T., Rugenstein, J.K.C., Ibarra, D.E., Winnick, M.J., Strömberg, C.A.E., and Chamberlain, C.P., 2022, Drier winters drove Cenozoic open habitat expansion in North America: AGU Advances, v. 3, e2021AV000566. https://doi.org/10.1029/2021AV000566

Latorre, C., Quade, J., and McIntosh, W.C., 1997, The expansion of C_4 grasses and global change in the late Miocene: Stable isotope evidence from the Americas: Earth and Planetary Science Letters, v. 146, p. 83–96. https://doi.org/10.1016/S0012-821X(96)00231-2

Licht, A., Dupont-Nivet, G., Meijer, N., Rugenstein, J.K.C., Schauer, A., Fiebig, J., Mulch, A., Hoorn, C., Barbolini, N., and Guo, Z., 2020, Decline of soil respiration in northeastern Tibet through the transition into the Oligocene icehouse: Palaeogeography, Palaeoclimatology, Palaeoecology, v. 560, 110016. https://doi.org/10.1016/j.palaeo.2020.110016

Machette, M.N., 1985, Calcic soils of the southwestern United States: Geological Society of America, Special Paper 203, p. 1–21. https://doi.org/10.1130/SPE203-p1

Mack, G.H., Cole, D.R., James, W.C., Giordano, T.H., and Salyards, S.L., 1994, Stable oxygen and carbon isotopes of pedogenic carbonate as indicators of Plio-Pleistocene paleoclimate in the southern Rio Grande rift, south-central New Mexico: American Journal of Science, v. 294, p. 624–640. https://doi.org/10.2475/ajs.294.5.621

Mankin, J.S., Smerdon, J.E., Cook, B.I., Williams, A.P., and Seager, R., 2017, The curious case of projected 21st-century drying but greening in the American West: Journal of Climate, p. JCLI-D-17-0213.1. https://doi.org/10.1175/JCLI-D-17-0213.1

Manser, L., Kukla, T., and Rugenstein, J.K.C., 2024, Stable isotope evidence for long-term stability of large-scale hydroclimate in the Neogene North American Great Plains: Climate of the Past, v. 20, p. 1039–1065. https://doi.org/10.5194/cp-20-1039-2024

Milly, P.C.D., and Dunne, K.A., 2020, Colorado River flow dwindles as warming-driven loss of reflective snow energizes evaporation: Science, v. 367, p. 1252–1255. https://doi.org/10.1126/science.aay9187

Min, K., Mundil, R., Renne, P.R., and Ludwig, K.R., 2000, A test for systematic errors in $^{40}Ar/^{39}Ar$ geochronology through comparison with U/Pb analysis of a 1.1-Ga rhyolite: Geochimica et Cosmochimica Acta, v. 41, p. 73–98. https://doi.org/10.1016/S0016-7037(99)00204-5

Mix, H.T., Winnick, M.J., Mulch, A., and Chamberlain, C.P., 2013, Grassland expansion as an instrument of hydrologic change in Neogene western North America: Earth and Planetary Science Letters, v. 377–378, p. 73–83. https://doi.org/10.1016/j.epsl.2013.07.032

Montañez, I.P., 2013, Modern soil system constraints on reconstructing deep-time atmospheric CO_2: Geochimica et Cosmochimica Acta, v. 101, p. 57–75. https://doi.org/10.1016/j.gca.2012.10.012

Overpeck, J.T., and Udall, B., 2020, Climate change and the aridification of North America: Proceedings of the National Academy of Sciences, v. 117, p. 11856–11858. https://doi.org/10.1073/pnas.2006323117

Quade, J., and Roe, L.J., 1999, The stable-isotope composition of early ground-water cements from sandstone in paleoecological reconstruction: Journal of Sedimentary Research, v. 69, p. 667–674. https://doi.org/10.2110/jsr.69.667

Quade, J., Cerling, T.E., and Bowman, J.R., 1989, Development of the Asian monsoon revealed by marked ecological shift during the latest Miocene in northern Pakistan: Nature, v. 342, p. 163–166. https://doi.org/10.1038/342163a0

Raich, J.W., and Schlesinger, W.H., 1992, The global carbon dioxide flux in soil respiration and its relationship to vegetation and climate: Tellus B, v. 44B, p. 81–99. https://doi.org/10.3402/tellusb.v44i2.15428

Rugenstein, J.K.C., and Chamberlain, C.P., 2018, The evolution of hydroclimate in Asia over the Cenozoic: A stable-isotope perspective: Earth-Science Reviews, v. 185, p. 1129–1156. https://doi.org/10.1016/j.earscirev.2018.09.003

Rugenstein, J.K.C., Methner, K., Kukla, T., Mulch, A., Lüdecke, T., Fiebig, J., Wegmann, K.W., Zeitler, P.K., and Chamberlain, C.P., 2022, Clumped isotope constraints on warming and precipitation seasonality in Mongolia following Altai uplift: American Journal of Science, v. 322, p. 28–54. https://doi.org/10.2475/01.2022.02

Schmidt, D.F., and Grise, K.M., 2021, Drivers of twenty-first century U.S. winter precipitation trends in CMIP6 models: A storyline-based approach: Journal of Climate, v. 34, p. 6875–6889. https://doi.org/10.1175/jcli-d-21-0080.1

Seager, R., and Vecchi, G.A., 2010, Greenhouse warming and the 21st century hydroclimate of southwestern North America: Proceedings of the National Academy of Sciences of the United States of America, v. 107, p. 21277–21282. https://doi.org/10.1073/pnas.0910856107

Sheppard, P.R., Comrie, A.C., Packin, G.D., Angersbach, K., and Hughes, M.K., 2002, The climate of the US Southwest: Climate Research, v. 21, p. 219–238. https://doi.org/10.3354/cr021219

Simpson, I.R., McKinnon, K., Davenport, F., Tingley, M., Lehner, F., Fahad, S., and Chen, D., 2021, Emergent constraints on the large-scale atmospheric circulation and regional hydroclimate: Do they still work in CMIP6 and how much can they actually constrain the future? Journal of Climate, v. 34, p. 6355–6377. https://doi.org/10.1175/JCLI-D-21-0055.1

Spaur, S., Koning, D.J., Heizler, M., Aby, S., Williamson, G., Knott, J.R., Acosta, R.P., and Rugenstein, J.K.C., 2025, The hydroclimate and environmental response to middle Miocene warming in the southwestern USA: Stable isotope evidence: Paleoceanography and Paleoclimatology, v. 40, p. e2024PA005056. https://doi.org/10.1029/2024PA005056

Steinthorsdottir, M., Coxall, H.K., de Boer, A.M., Huber, M., Barbolini, N., Bradshaw, C.D., Burls, N.J., Feakins, S. J., Gasson, E., Henderiks, J., Holbourn, A.E., Kiel, S., Kohn, M.J., Knorr, G., Kürschner, W.M., Lear, C.H., Liebrand, D., Lunt, D.J., Mörs, T., Pearson, P.N., Pound, M.J., Stoll, H., and Strömberg, C.A.E., 2021, The Miocene: The future of the past: Paleoceanography and Paleoclimatology, v. 36, p. e2020PA004037. https://doi.org/10.1029/2020PA004037

Strong, M., Sharp, Z.D., and Gutzler, D.S., 2007, Diagnosing moisture transport using D/H ratios of water vapor: Geophysical Research Letters, v. 34, L03404. https://doi.org/10.1029/2006GL028307

Takeuchi, A., Hren, M.T., Smith, S.V., Chamberlain, C.P., and Larson, P.B., 2010, Pedogenic carbonate carbon isotopic constraints on paleoprecipitation: Evolution of desert in the Pacific Northwest, USA, in response to topographic development of the Cascade Range: Chemical Geology, v. 277, p. 323–335. https://doi.org/10.1016/j.chemgeo.2010.08.015

Tedford, R.H., and Barghoorn, S.F., 1999, Santa Fe Group (Neogene), Ceja del Rio Puerco, northwestern Albuquerque Basin, Sandoval County, New Mexico, *in* New Mexico Geological Society, Guidebook 50, p. 327–335. https://doi.org/10.56577/ffc-50.327

Tedford, R.H., Albright, L.B., Barnosky, A.D., Ferrusquia-Villafranca, I., Hunt, R.M., Storer, J.E., Swisher, C.C., Voorhies, M.R., Webb, S.D., and Whistler, D.P., 2004, Mammalian biochronology of the Arikareean through Hemphillian interval (late Oligocene through early Pliocene epochs), *in* Woodburne, M.O., ed., Late Cretaceous and Cenozoic Mammals of North America: New York, Columbia University Press, p. 169–231. https://doi.org/10.7312/wood13040-008

Tipple, B.J., Meyers, S.R., and Pagani, M., 2010, Carbon isotope ratio of Cenozoic CO_2: A comparative evaluation of available geochemical proxies: Paleoceanography, v. 25, PA3202. https://doi.org/10.1029/2009PA001851

Tulley-Cordova, C.L., Putman, A.L., and Bowen, G.J., 2021, Stable isotopes in precipitation and meteoric water: Sourcing and tracing the North American monsoon in Arizona, New Mexico, and Utah: Water Resources Research, v. 57, p. 32021WR030039. https://doi.org/10.1002/essoar.10506650.2

Ukkola, A.M., Prentice, I.C., Keenan, T.F., Dijk, A.I.J.M. van, Viney, N.R., Myneni, R.B., and Bi, J., 2016, Reduced streamflow in water-stressed climates consistent with CO_2 effects on vegetation: Nature Climate Change, v. 6, p. 75–78. https://doi.org/10.1038/nclimate2831

Wagner, J.D.M., Cole, J.E., Beck, J.W., Patchett, P.J., Henderson, G.M., and Barnett, H.R., 2010, Moisture variability in the southwestern United States linked to abrupt glacial climate change: Nature Geoscience, v. 3, p. 110–113. https://doi.org/10.1038/ngeo707

Westerhold, T. et al., 2020, An astronomically dated record of Earth's climate and its predictability over the last 66 million years: Science, v. 369, p. 1383–1388. https://doi.org/10.1126/SCIENCE.ABA6853

Wheeler, H.E., 1964, Baselevel, lithosphere surface, and time-stratigraphy: Geological Society of America Bulletin, v. 75, p. 599–609. https://doi.org/10.1130/0016-7606(1964)75[599:BLSAT]2.0.CO;2

Williamson, G.R., and Sweet, D.E., 2024, Composite stratigraphic section across the mid-Miocene climatic optimum and transition in the Tesuque Formation, Española Basin, north-central New Mexico: The Mountain Geologist, v. 61, p. 259–278. https://doi.org/10.31582/rmag.mg.61.4.259

Winnick, M.J., Welker, J.M., and Chamberlain, C.P., 2013, Stable isotopic evidence of El Niño-like atmospheric circulation in the Pliocene western United States: Climate of the Past, v. 9, p. 903–912. https://doi.org/10.5194/cp-9-903-2013

Wostbrock, J.A.G., Brand, U., Coplen, T.B., Swart, P.K., Carlson, S.J., Brearley, A.J., and Sharp, Z.D., 2020, Calibration of carbonate-water triple oxygen isotope fractionation: Seeing through diagenesis in ancient carbonates: Geochimica et Cosmochimica Acta, v. 288, p. 369–388. https://doi.org/10.1016/j.gca.2020.07.045

Yang, Y., Donohue, R.J., McVicar, T.R., and Roderick, M.L., 2015, An analytical model for relating global terrestrial carbon assimilation with climate and surface conditions using a rate limitation framework: Geophysical Research Letters, v. 42, p. 9825–9835. https://doi.org/10.1002/2015GL066835.

Appendices can be found at
https://nmgs.nmt.edu/repository/index.cfml?rid=2026005



View of Albuquerque from the northern Sandia Mountains. High mountains are not generally where one finds fossils. But at Tree Spring, in the southern part of the mountains, three teeth of the American mastodon, *Mammut americanum*, were discovered at 2,582 m (8,470 ft) elevation. This occurrence combined with two other high-elevation sites in Colorado and Utah implies that *M. americanum* occupied montane habitats during occupied montane habitats during late Pleistocene time. Photograph courtesy of “Celestyn Brożek.